Center for Environmentally Sustainable Transportation in Cold Climates

A Bio-Wicking System to Prevent Frost Heave in Alaskan Pavements: Phase II-Implementation

Javad Galinmoghadam, Graduate Research Assistant
Xiong Zhang, Ph.D., P.E.
Chuang Lin, Ph.D.

Department of Civil, Architectural, and Environmental Engineering
Missouri University of Science and Technology

Date: November 2019

INE/CESTiCC 19.29

Prepared by: Xiong Zhang

Center for Environmentally Sustainable Transportation in Cold Climates (CESTiCC)
Duckering Building, Room 245
P.O. Box 755900
Fairbanks, AK 99775

REPORT DOCUMENTATION PAGE

Form approved OMB No.

1. AGENCY USE ONLY (LEAVE BLANK)	2. REPORT DATE	3. REPORT TYPE AND DATES COVERED
	11/2016	Final Report: 06/2014 – 12/2016

4. TITLE AND SUBTITLE

A Bio-Wicking System to Prevent Frost Heave in Alaskan Pavements: Phase II - Implementation

5. FUNDING NUMBERS

6. AUTHOR(S)

Javad Galinmoghadam, Graduate Research Assistant
Xiong Zhang, Ph.D., P.E.
Chuang Lin, Ph.D.
Missouri University of Science and Technology

7. PERFORMING ORGANIZATION NAME(S) AND ADDRESS(ES)

Center for Environmentally Sustainable Transportation in Cold Climates
University of Alaska Fairbanks
Duckering Building, Room 245
P.O. Box 755900
Fairbanks, AK 99775-5900

8. PERFORMING ORGANIZATION REPORT NUMBER

INE/CESTiCC 19.29

9. SPONSORING/MONITORING AGENCY NAME(S) AND ADDRESS(ES)

TenCate Geosynthetics
365 South Holland Drive
Pendergrass, GA 30567

U.S. Department of Transportation
1200 New Jersey Avenue, SE
Washington, DC 20590

10. SPONSORING/MONITORING AGENCY REPORT NUMBER

11. SUPPLEMENTARY NOTES

12a. DISTRIBUTION / AVAILABILITY STATEMENT

No restrictions

12b. DISTRIBUTION CODE

13. ABSTRACT (Maximum 200 words)

Water within pavement layers is the major cause of pavement deterioration. High water content results in significant reduction in soil's resilient behavior and an increase in permanent deformation. Especially in cold regions, frost heave and thaw weakening cause extensive damage to roads and airfields. Conventional drainage systems can only drain gravity water not capillary water. Both preliminary lab and field tests have proven the drainage efficiency of a newly developed H2Ri geotextile with wicking fabrics.

In this report, continuous research was conducted to verify the effectiveness of the wicking fabric in mitigating frost boil issues in Alaskan pavemnets. Two test sections were selected at two low volume roads on the campus of the University of Alaska Fairbanks. Soil moisture and temperature sensors were installed within the road embankments. The monitored data was used to analyze the soil migrations and evaluate the drainage performance of the wicking fabric. Preliminary monitoring results showed that the wicking fabric was effective in mitigating the frost boil problem.

14- KEYWORDS: Geotextiles, Subsurface Drainage, Unsaturated Soils, Pavement, frost heave, and thaw weakening

15. NUMBER OF PAGES

67

16. PRICE CODE

N/A

17. SECURITY CLASSIFICATION OF REPORT	18. SECURITY CLASSIFICATION OF THIS PAGE	19. SECURITY CLASSIFICATION OF ABSTRACT	20. LIMITATION OF ABSTRACT
Unclassified	Unclassified	Unclassified	N/A

A Wicking System to Prevent Frost Heave in Alaskan Pavements:

Phase II – Implementation

Project Report

By

Javad Galinmoghadam
Graduate Research Assistant

Xiong Zhang, Ph.D., P.E.
Associate Professor

Chuang Lin, Ph.D.

Department of Civil, Architectural, and Environmental Engineering

Missouri University of Science and Technology

Project Title: A Wicking System to Prevent Frost Heave in Alaskan Pavements:

Phase II - Implementation

Performed in cooperation with

TenCate Geosynthetics (North America)

November 2019

DISCLAIMER

This document is disseminated under the sponsorship of the U.S. Department of Transportation in the interest of information exchange. The U.S. Government assumes no liability for the use of the information contained in this document. The U.S. Government does not endorse products or manufacturers. Trademarks or manufacturers' names appear in this report only because they are considered essential to the objective of the document.

Opinions and conclusions expressed or implied in the report are those of the author(s). They are not necessarily those of the funding agencies. This report does not constitute a standard, specification, or regulation.

METRIC (SI*) CONVERSION FACTORS

APPROXIMATE CONVERSIONS TO SI UNITS

Symbol	When You Know	Multiply By	To Find	Symbol
		LENGTH		
in	inches	25.4		mm
ft	feet	0.3048		m
yd	yards	0.914		m
mi	Miles (statute)	1.61		km
		AREA		
in^2	square inches	645.2	millimeters squared	cm^2 ft^2
	square feet	0.0929	meters squared	m^2
yd^2	square yards	0.836	meters squared	m^2
mi^2	square miles	2.59	kilometers squared	km^2
ac	acres	0.4046	hectares	ha
		MASS (weight)		
oz	Ounces (avdp)	28.35	grams	g lb
	Pounds (avdp)	0.454	kilograms	kg T
	Short tons (2000 lb)	0.907	megagrams	mg
		VOLUME		
fl oz	fluid ounces (US)	29.57	milliliters	mL gal
	Gallons (liq)	3.785	liters	liters ft^3
	cubic feet	0.0283	meters cubed	m^3
yd^3	cubic yards	0.765	meters cubed	m^3
Note: Volumes greater than 1000 L shall be shown in m^3				
		TEMPERATURE (exact)		
ºF temperature	Fahrenheit	5/9 (ºF-32)	Celsius temperature	ºC
		ILLUMINATION		
fc	Foot-candles	10.76	lux	lx
fl	foot-lamberts	3.426	candela/m^2	cd/cm^2
		FORCE and PRESSURE or STRESS		
lbf	pound-force	4.45	newtons	N psi
square inch	pound-force per	6.89	kilopascals	kPa

These factors conform to the requirement of FHWA Order 5190.1A *SI is the symbol for the International System of Measurements

APPROXIMATE CONVERSIONS FROM SI UNITS

Symbol	When You Know	Multiply By	To Find	Symbol
		LENGTH		
mm	millimeters			0.039
inches			in	
m	meters			3.28
feet			ft	
m	meters			1.09
yards			yd	
km	kilometers			0.621
Miles (statute)			mi	
		AREA		
mm^2	millimeters squared			0.0016 square inches
in^2 m^2	meters squared			10.764 square
feet			ft^2 km^2	kilometers squared
0.39	square miles		mi^2 ha	hectares
(10,000 m^2)			2.471	acres
ac				
		MASS (weight)		
g	grams			0.0353
Ounces (avdp)			oz	
kg	kilograms			2.205
Pounds (avdp)			lb mg	megagrams (1000 kg)
1.103	short tons		T	
		VOLUME		
mL	milliliters			0.034
fluid ounces (US)			fl oz	
liters	liters			0.264
Gallons (liq)			gal	
m^3	meters cubed			35.315
cubic feet			ft^3	
m^3	meters cubed			1.308
cubic yards			yd^3	
		TEMPERATURE (exact)		
ºC	Celsius temperature			9/5 ºC+32
Fahrenheit temperature			ºF	
		ILLUMINATION		
lx	lux			0.0929
foot-candles			fc	
cd/cm	candela/m^2			0.2919

ACKNOWLEDGMENTS

The authors wish to express their appreciation to TenCate Geosynthetics (North America) and the Center for Environmentally Sustainable Transportation in Cold Climates (CESTiCC) for their financial support throughout this study. The authors would also like to thank all members of the project advisory committee.

TABLE OF CONTENTS

LIST OF FIGURES

EXECUTIVE SUMMARY

Alaskan pavements have suffered from the frost boil problem for decades and conventional treatments have been proven to be not effective in mitigating the frost boil problem. The previous project, entitled “A Bio-Wicking System to Mitigate Capillary Water in Base Coarse”, proved the effectiveness of the bio-wicking system in draining both capillary and free water out of a typical base coarse aggregate (E-1). Both elemental level and full-scale tests showed that the boil-wicking system efficiently dehydrated road embankment under unsaturated conditions. However, the tests performed in the previous project were conducted in a relatively well-controlled environment. Moreover, the testing system consisted of a single layer of base coarse aggregate and the drainage performance of the H2Ri wicking fabric in a roadway system still required further evaluation.

This project aimed at further verifying the effectiveness of the H2Ri wicking fabric in mitigating the frost boil problem. Two field test sections, one an unpaved road and the other a paved road, were selected on campus at the University of Alaska Fairbanks. Within each test section, soil moisture and temperature sensors were installed within the subgrade, subbase, and base course layers. The pavement drainage performance for the areas with and without the H2Ri wicking fabric was monitored and compared. The preliminary monitoring results at test section I, Georgeson Botanical Garden, indicated that the wicking fabric was effective in reducing the soil water content. The soil water content quickly decreased for the testing area installed with the wicking fabric. The construction of test section II, Toklat Way, was postponed to the summer of 2019. Insufficient data is available to perform the analysis, therefore no conclusive results are present at the moment of composing this report.

CHAPTER 1: INTRODUCTION

1.1 Problem Statement

Frost heave and thaw weakening cause extensive damage to roads and airfields in cold regions. Government transportation engineers in cold regions have credited a minimum of half of road maintenance expenditures to the effects of freezing and thawing (Henry and Holtz, 2001). The three elements necessary for ice lenses and thus frost heave are (1) frost susceptible (FS) soil, (2) subfreezing temperatures, and (3) capillary water (must be available from the groundwater table, infiltration, an aquifer, or held within the voids of fine-grained soil). Removal any of the three conditions above will eliminate or at least minimize frost heave and thaw weakening. Unfortunately, all three conditions are met in many places of interior Alaska. A conventional drainage system relies on gravity to drain water out of soils ((Henry and Holtz, 2001); (Cedergren, 1994); (Christopher *et al.*, 1997)), which cannot drain the capillary water and prevent the frost heave and thaw weakening from happening. Consequently, frost heave and thaw weakening cause extensive damages to pavement structures in interior Alaska.

The H2Ri wicking fabric, which is newly developed by TENCATE GEOSYNTHETICS, shows great promise as a cost-effective means of controlling moisture migration and mitigating the frost heave and subsequent thaw weakening. Available data and field observations at different applications have clearly indicated that H2Ri wicking fabric has successfully facilitated the road construction, eliminated the frost boil problem in the test section, and resulted in significant cost savings. In a recently completed Center for Environmentally Sustainable Transportation in Cold Climates (CESTiCC) project entitled “A Bio-Wicking System to Prevent Frost Heave in Alaskan Pavements,” elementary box and flume tests were used to evaluate if the

bio-wicking system can be used to address the above concerns. Preliminary results from the previous project indicate that bio-wicking is a feasible way to resolve the potential concerns in the use of H2Ri wicking fabric to mitigating the frost heave and thaw weakening. However, the research project was based on the elemental level and full-scale physical model test. The tests were conducted under a relatively well controlled condition, which was not a representative in-situ condition. Therefore, it is necessary to further evaluate the effectiveness of the H2Ri wicking fabric in the field.

1.2 Research Objective and Methodology

The objective of this research was to continue evaluating the effectiveness of the bio-wicking system to mitigate frost heave in a real-world scenario. Two locations, Yukon Drive (unpaved road) and Tolkat Drive (paved road) were selected as the test sections. Soil moisture and temperature sensors were implemented in the test section to continuously monitor water migration within the test sections with and without the H2Ri wicking fabric. The test sections were planned to be monitored for 2 years and the monitored results analyzed to evaluate the effectiveness and efficiency of the H2Ri wicking fabric in terms of mitigating the frost boil issue.

1.3 Scope of Study

To achieve the research objectives, the project aimed to accomplish the following tasks:

Task 1: Literature Review

Task 1 involved a comprehensive literature search on frost heave issues. The ongoing research regarding the cause and rehabilitation of frost heave problems was studied. In addition,

the existing laboratory study and field applications of the H2Ri wicking fabric to mitigate the frost boil issue were evaluated. Task 1 provided useful information on the current state of art of the engineering applications of the wicking fabric in mitigating the frost boil issue.

Task 2: Test Design

Task 2 included the designs of the field test sections for the selected paved and unpaved road. Firstly, the pavement structures of the test section will be presented and the installation location of the H2Ri wicking fabric will be demonstrated. Secondly, the distributions of soil temperature and moisture sensors will be provided. Thirdly, the drainage system of each test section will be discussed in detail.

Task 3: Construction

Task 3 is to perform the construction strictly in accordance with the test designs.

Task 4: Data Analysis and Draft of Final Report

Task 4 comprehends the completion of a final report on Task 1 through 3. The results from those three tasks are synthesized and analyzed to evaluate the effectiveness of the H2Ri wicking fabric in mitigating frost boil issues. Recommendations will be provided for future engineering applications in related scenarios.

CHAPTER 2: LITERATURE REVIEW

Frost heave and thaw weakening cause extensive damage to roads and their pavements in cold regions when the 3 conditions of (a) frost susceptible soil, (b) water, and (c) freezing temperature are met. Frost heave is the result of the gradual formation of ice lenses in freezing temperature below the pavement. Figure 2.1 shows the procedure that results in forming ice lenses below the pavement.

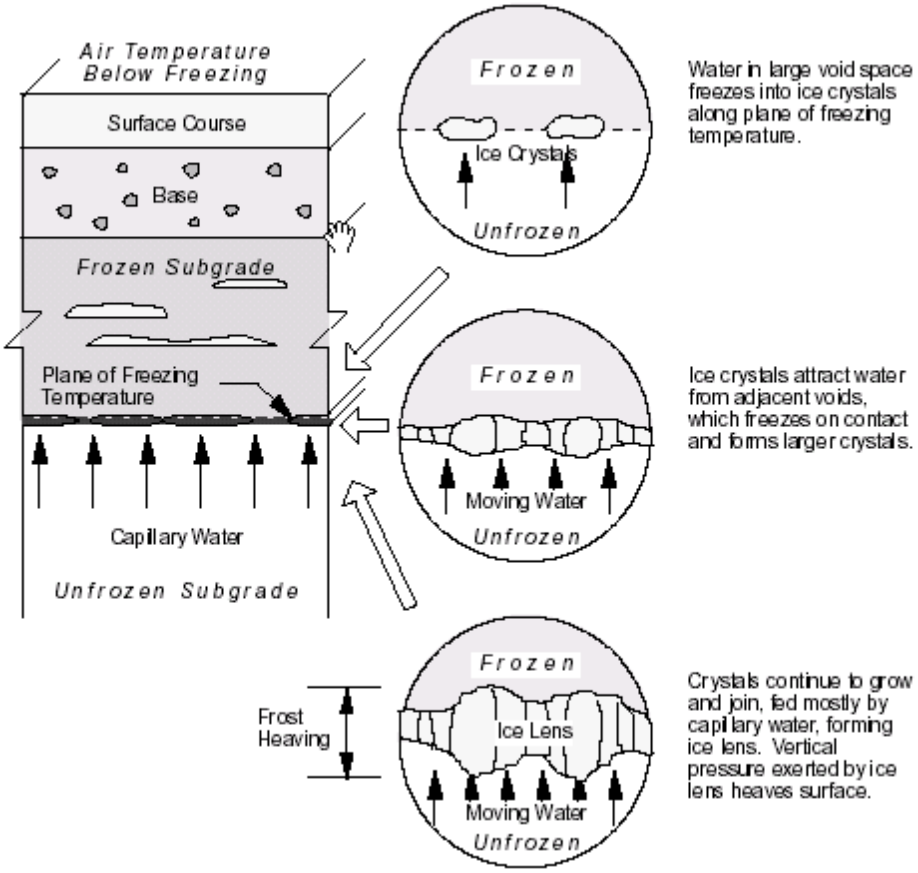

Figure 2.1 Formation of ice lenses (Zhang and Presler, 2012)

Several techniques have been proposed to reduce the unwanted effects of frost heave. Carlson and Nixon studied the effect of frost heave in a buried pipeline. They found that both increasing the depth of burial and replacing the silty soil with granular material reduce the amount of frost heave and thaw settlement (Carlson and Nixon, 1988). Henry performed a

laboratory test to study the capillary break effect of certain geotextiles to reduce frost heave (Henry, 1990). He showed that using one layer of geotextile can reduce frost heave up to 70% based on different soil types. He also concluded that the fabric works best if it is placed between the water table and frost penetration depth. He also mentioned that surface chemical properties of geotextile can affect its performance in reducing frost heave. In a later study, he concluded that the combined effect of reinforcement, separation and filtration of geotextiles along its capillary barrier effect due to its pore size distribution can contribute to reducing frost heave and thaw weakening adverse effects (Henry, 1996). In another study, a new kind of embankment structure, which consists of geotextile, crushed-rock layer and geomembrane, was designed to mitigate frost heave, frost boils and thawing settlement with traditional crushed-rock layer only. The structure was investigated both in the laboratory and the field at Budongquan located at Qinghai–Tibet Plateau (Lai, Zhang and Yu, 2012). They showed that using the combination of geotextile, crushed-rock, and geomembrane is more effective than using only crushed-rock as a capillary barrier. Using a capillary barrier reduces the water as a key factor for inducing frost heave. Another way of dealing with this issue is reducing the susceptibility of the soil, either by replacing it with a less susceptible soil or improving its characteristics. It has been shown that addition of up to 15% type C fly ash (per ASTM 2003) Portland cement would reduce the susceptibility of the subgrade and subbase to a very low value.(Zhang, Johnson and White, 2016).

In recent years, a new type of wicking fabric (H2Ri) was developed by TenCate Geosynthetics to remove the capillary water in the pavement structure and potentially maintain good pavement performance and longevity. The wicking fabric is made of a special type of hydrophilic Nylon fibers with multichannel cross-sections. Figure 2.2(a) shows the top view of

the wicking fabric. 0(b) shows the scanning electron microscopy (SEM) photo of multiple fibers and a single fiber at different magnification ratios, respectively. The multichannel cross-section has a high shape factor and a great number of channels per fiber (specific surface area = 3650 cm^2/g), which give the wicking fabric great potential for maximizing capillary action and water transport in an unsaturated environment.

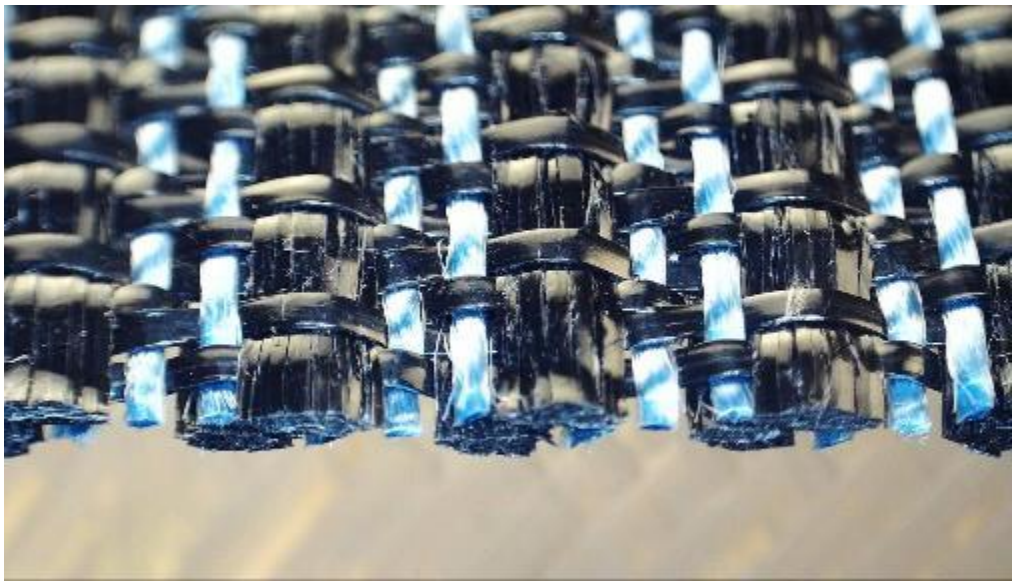

(a) H2Ri wicking fabric

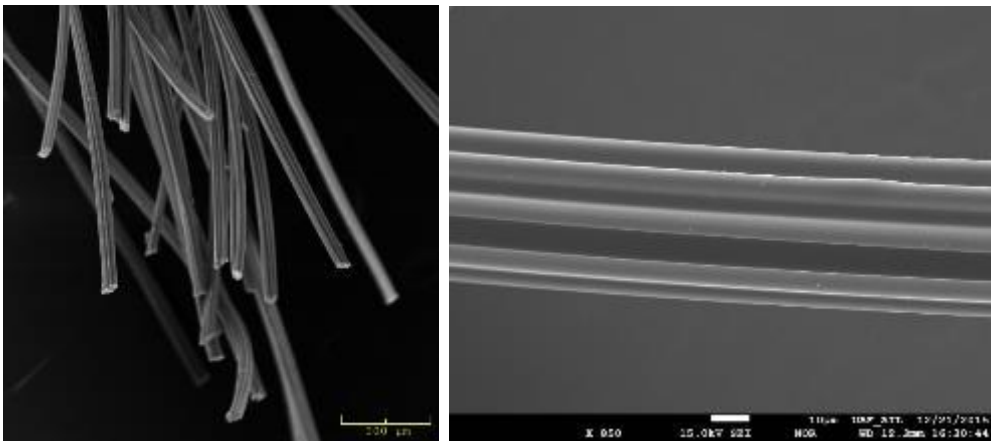

(b) SEM image of wicking fibers

Figure 2.2 H2Ri wicking fabric

The effectiveness of the H2Ri wicking fabric in dehydrating road embankment has been systematically studied via laboratory and field tests. For example, Zhang and Belmont (2012)

compared the drainage efficiency of the H2Ri wicking fabric together with other traditional geotextiles and concluded that the wicking fabric could potentially be used as a capillary barrier to mitigate frost heave problems. In 2010, Zhang et al. (2014) selected a test section on Dalton Highway to evaluate the effectiveness of the wicking fabric to prevent frost boils and the test results were satisfactory. Lin et al. (2017) continuously monitored the field performance of the wicking fabric and indicated that frost boil problem was eliminated. In a recently completed CESTiCC project (Lin and Zhang, 2016) entitled "A Bio-Wicking System to Prevent Frost Heave in Alaskan Pavements", elementary box and flume tests were used to evaluate if the bio-wicking system can be used to address the above concerns. Preliminary results from the previous project indicate that bio-wicking is a feasible way to resolve the potential concerns in the use of H2Ri wicking fabric to mitigating the frost heave and thaw weakening. However, the tests performed in this project was relatively well-controlled and might not represent the field condition. Therefore, this paper focuses on evaluating the in-situ performance of the H2Ri wicking fabric and determining the effectiveness of the H2Ri wicking fabric in a bio-wicking system in the real-world scenarios.

CHAPTER 3: TEST DESIGNS AND CONSTRUCTION PROCESSES

This chapter describes the design and construction processes of two test sections. One test section was selected to be at the Yukon Drive near the Georgeson Botanical Garden at the University of Alaska Fairbanks. The roadway was unpaved and two areas were chosen to be rehabilitated on the west and east sides, respectively. The other test section was selected to be at the Toklat Way, which was north of the Reichardt Building and south of North Tanana Loop. The road was paved and suffered from frost boils due to poor soil conditions. Both of the test sections were treated with the H2Ri wicking fabric. Soil temperature and moisture sensors will be monitored for two years to verify the effectiveness of H2Ri to mitigate frost boils in both unpaved and paved roadways in Alaska.

3.1 Test Section I – Georgeson Botanical Garden

Test Section Introduction

Figure 3.1 shows the top view of the Yukon Drive, the first test section located at the southwest of the Georgeson Botanical Garden. The red line in Figure 3.1 shows the centerline of the Yukon Drive and the corresponding elevations are presented at the bottom of the figure. The northside of the Yukon Drive has a higher elevation compared to the west and east sides. The average slopes on the west and east sides of the roadway were +8.9% (upward to the north) and -5.3% (downward to the south), respectively. In early spring and summer, melting snow and water would flow from the north sides of the road to the west and east sides where soft spots were observed. To verify the effectiveness of the H2Ri wicking fabric, two areas were selected where excess water was expected to accumulate.

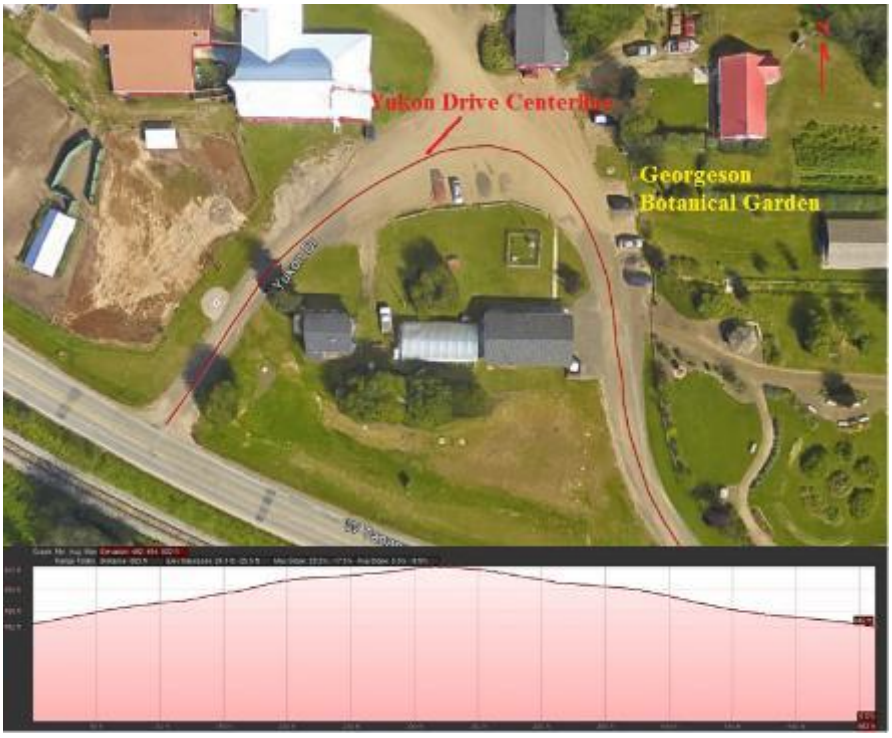

Figure 3.1 Test Section I: Yukon Drive near Georgeson Botanical Garden (Google Inc., 2011)

Test Design

Figure 3.2 shows the selected two testing areas, one on the west side and the other one on the east side of the Yukon Drive. For the test section on the west side, the red dash line represented the original test area. However, due to the budget limit, the testing area on the west side was finalized to be 29 ft. wide and 75 ft. long and the H2Ri wicking fabric would be installed on top of the subgrade (or in-situ soil). Two locations (cross sections 1 and 2) were selected to install soil moisture and temperature sensors and detailed sensor layout designs will be demonstrated in the following section. The wirings of the sensors were collected and mounted to the data collection station on the east side of the test area (yellow cube in Figure 3.2). On the east side of the Yukon Drive, another test area was chosen. The width of the test area was 29 ft., same as the test area on the west side. However, 15 ft. of the 75 ft-long test area did not have the H2Ri wicking fabric installed and was considered the control section. Moreover, two locations

within the untreated and treated areas (cross sections 3 and 4) were selected to install sensors. The wirings of the sensors were also collected and mounted to the data collection station located on the west side of the test area.

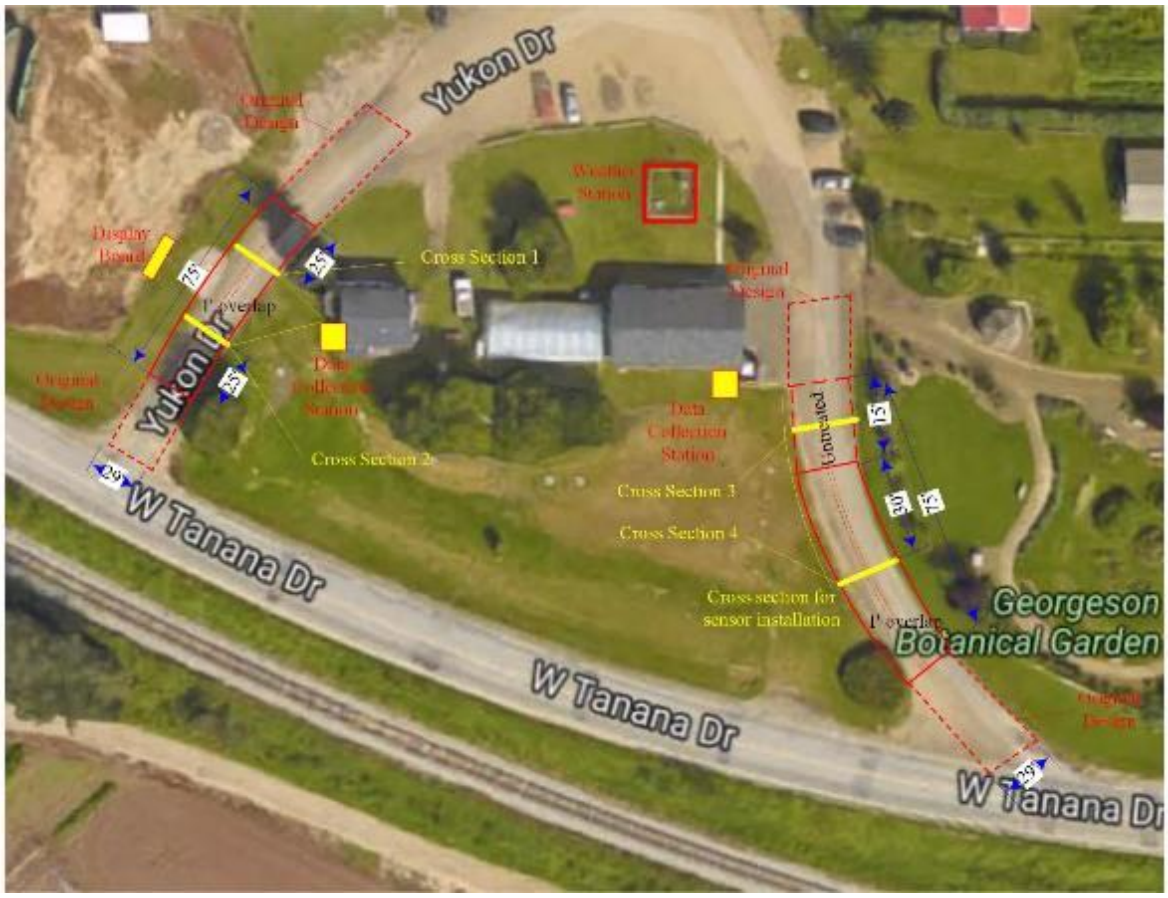

Figure 3.2 Layout of test areas

Figure 3.3 shows the sensor layout for Cross Sections 1-4. Figure 3.3 (a) shows the soil profile and the proposed sensor locations for Cross Sections 1 and 2 that on the west test area. The dash lines represented the proposed cutting lines. The proposed clearing and grading width of the subgrade was 28 ft. The roadway consisted of a 6-in. thick RAP (Reclaimed Asphalt Pavement) layer and a 12-in. thick Type A Fill, from the top to the bottom. The H2Ri wicking fabric would be installed on top of the subgrade soil. The proposed installation gradient was 2º, with the west end higher than the east end. Since each roll of the H2Ri wicking fabric was 15 ft.

in width, two rolls should be used with a minimum of 1 ft. overlap. On the west side, the H2Ri wicking fabric was tilting upward in parallel with the excavation line. On the east side, a 3-in. diameter drainage pipe was proposed to collect the excess water drained by the H2Ri wicking fabric. The east side of the wicking fabric was installed in a shingle style, as shown in Figure 3.4. Since the H2Ri wicking fabric has a stronger drainage ability along the weaving direction of the wicking fiber, the wicking fabric shall be such installed that the wicking fibers were along the transverse direction, as shown in Figure 3.4(a). As the excess water flowed to the edge of the roadway, the wicking fabric was rotated 90º to ensure the excess water flow from north (with a higher elevation) to south (with a lower elevation), as shown in Figure 3.4(b). In total, 15 sensors were distributed into 3 layers within each cross section. The first layer of sensors was to be installed 6 in. below the subgrade. The second layer of sensors was installed 2 in. above the wicking fabric. The third layer of sensors was installed 1 in. from the top of the Type A fill.

Figure 3.3(b) shows the soil profile and sensor layout for Cross Section 3 on the east test area of the Yukon Drive. This test area was the control section without the H2Ri wicking fabric. The sensor layout in Cross Section 3 is similar to that in Cross Sections 1 and 2. Figure 3.3(c) shows the soil profile and sensor layout for Cross Section 4 in which the H2Ri wicking fabric was installed. Different from the design on the west side, both ends of the H2Ri wicking fabric were inserted into a 3-in. diameter drainage pipe. Besides this, the sensor distributions in Cross Section 4 were the same as those in Cross Section 3. Figure 3.5 further shows the design of the drainage pipe. There shall be at least a 6-in. overlap for the H2Ri wicking fabric. The wicking fabric was sandwiched by two layers of woven geotextile to prevent contamination. The 3-in. diameter HDPE drainage pipe was buried 12 in. below the subgrade and the excess H2Ri wicking fabric was stuffed into the pipe to prevent from yanking out.

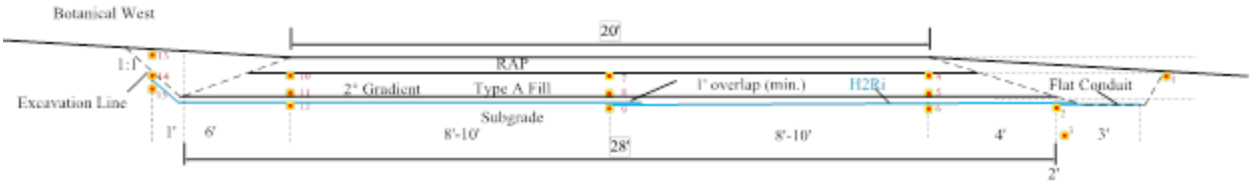

(a) Cross Sections 1 and 2 (West side)

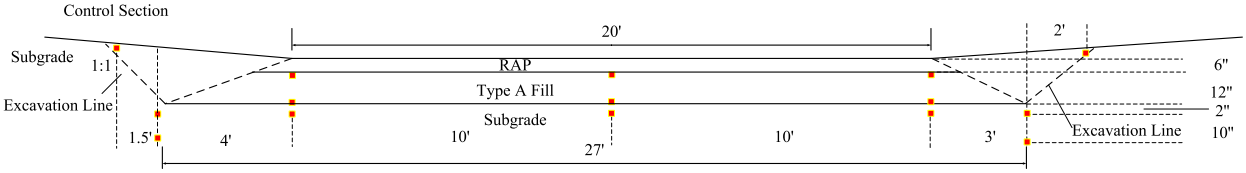

(b) Cross Section 3 (East side, untreated)

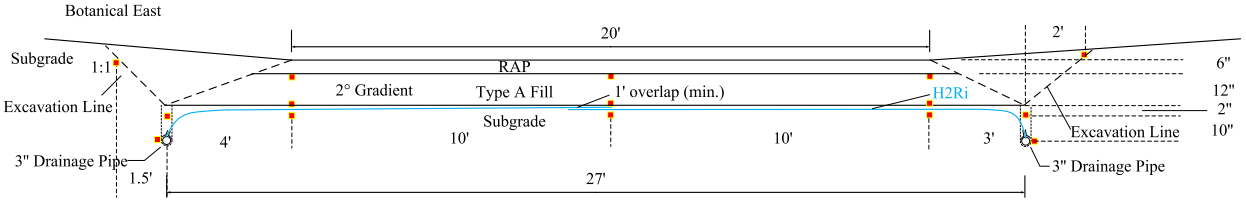

(c) Cross Section 4 (east side, treated)

Figure 3.3 Soil profiles and sensor layouts for Cross Sections 1-4

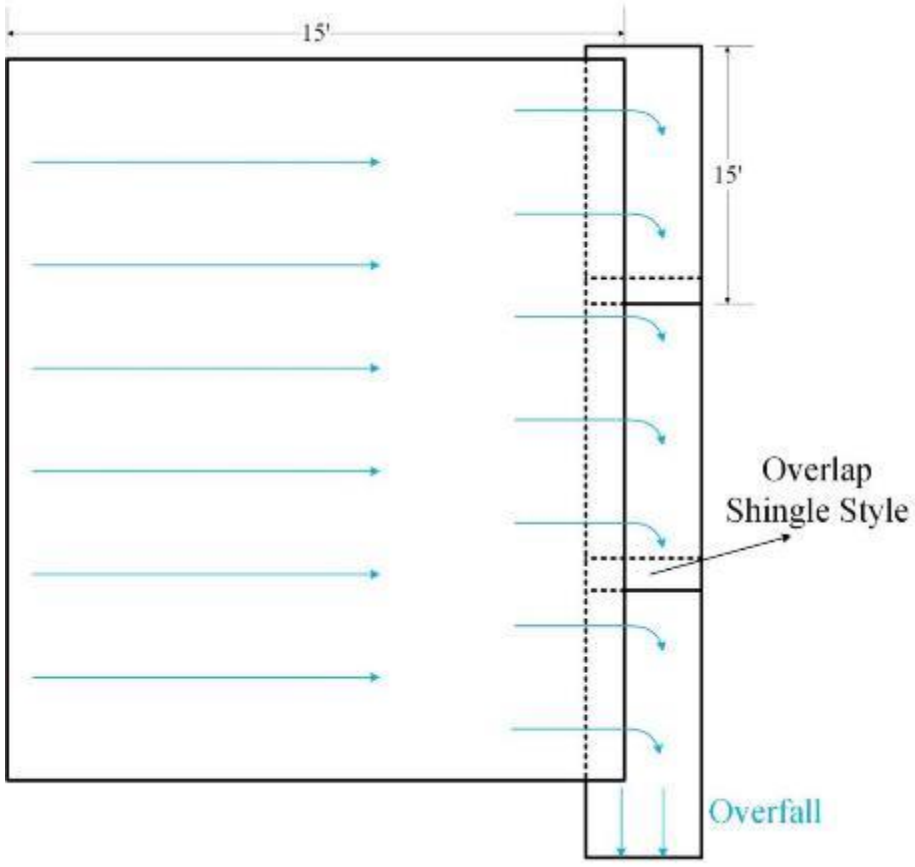

(a) Top view

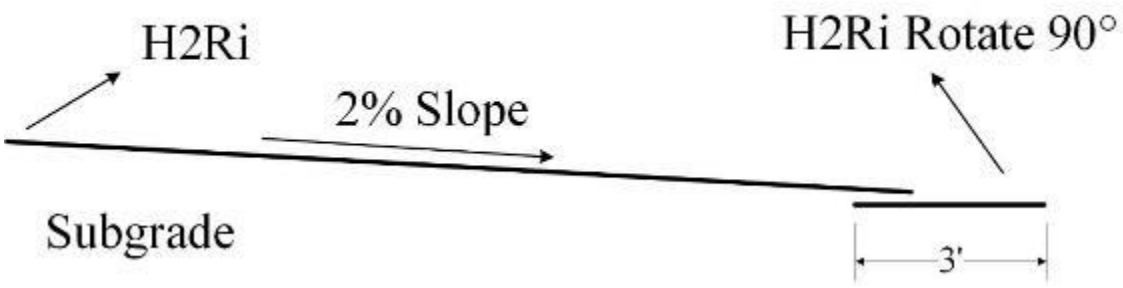

(b) front view

Figure 3.4 Shingle style overlap design (Cross Sections 1 and 2)

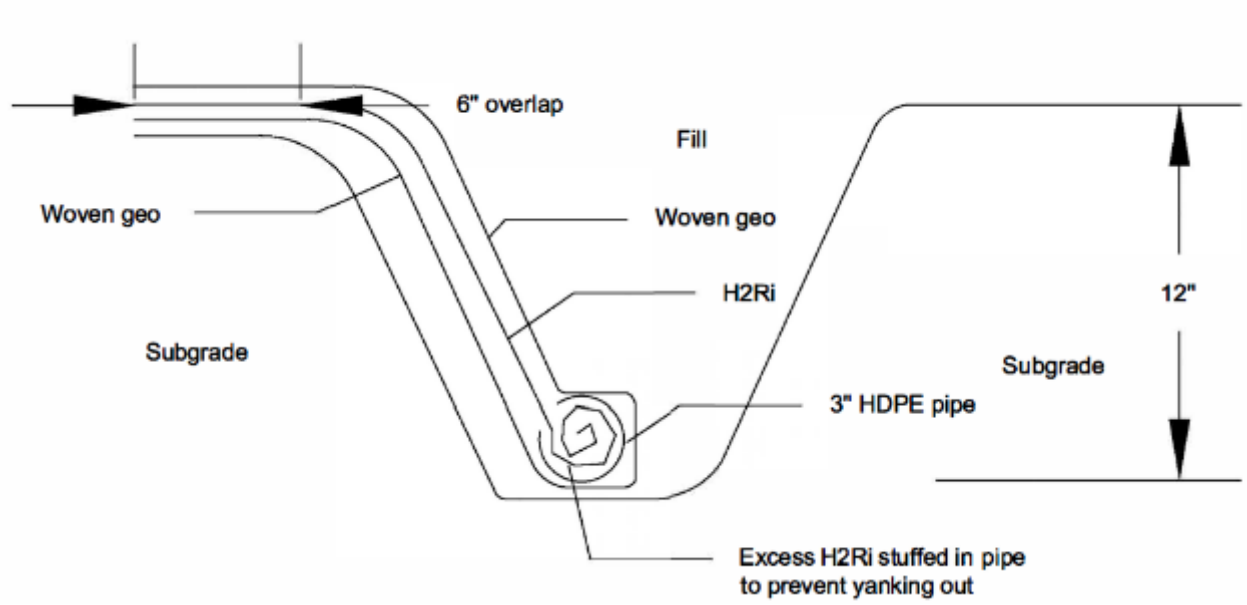

Figure 3.5 Drainage pipe design (Cross Section 4)

Construction Process

The construction phase of Test Section I started on September 20, 2017 and lasted for four days. The construction work was contracted to Weber Inc. and commenced at the west test area, as shown in Figure 3.6. The topsoil was first removed and the excavation depth was 24 in. During the excavation process, old woven geotextile debris from previous rehabilitation was observed, indicating that the traditional woven geotextile was not effective in dealing with frost boil issues. During the excavation process, the subgrade soil was graded to a 2% grade from west to east so that water flowed to the exit at the southeast corner of the excavation. The excavation

depth was measured and controlled by a GPS device and ranged from 24 in. to 26 in. The final excavation length was 75 ft., and a width of 21 ft. on the north side and 18 ft. on the south side.

Figure 3.6 Excavation of the test section on the west side

Figure 3.7(a) shows the determination of the cross sections 1 and 2. After the excavation had been completed, the Cross Section 2, which was 25 ft. north of the edge of west test area, was determined and marked. Then, the Cross Section 1, which was 25 ft. north of Cross Section 2, was also marked. After that, the locations of the first layer of sensors were determined. A shovel was used to dig a 6-in. deep hole into the subgrade soil and a GPS device was used to check the buried depth, as shown in Figure 3.7(b).

(a)

(b)

Figure 3.7 Determination of Cross Sections 1 and 2

Figure 3.8 shows the sensor installation procedure. The ECH_2O EC-5 VWC sensor was used to monitor the soil volumetric water content variations. The sensor has a functional range

was 0%-100% with a resolution of 0.001 m^3/m^3. The average accuracy of the sensor was ±2~3 %. Due to the inconsistency of the subgrade soil, uniform sand was used to backfill the hole so that the sensor readings could be expected to be consistent and comparable.

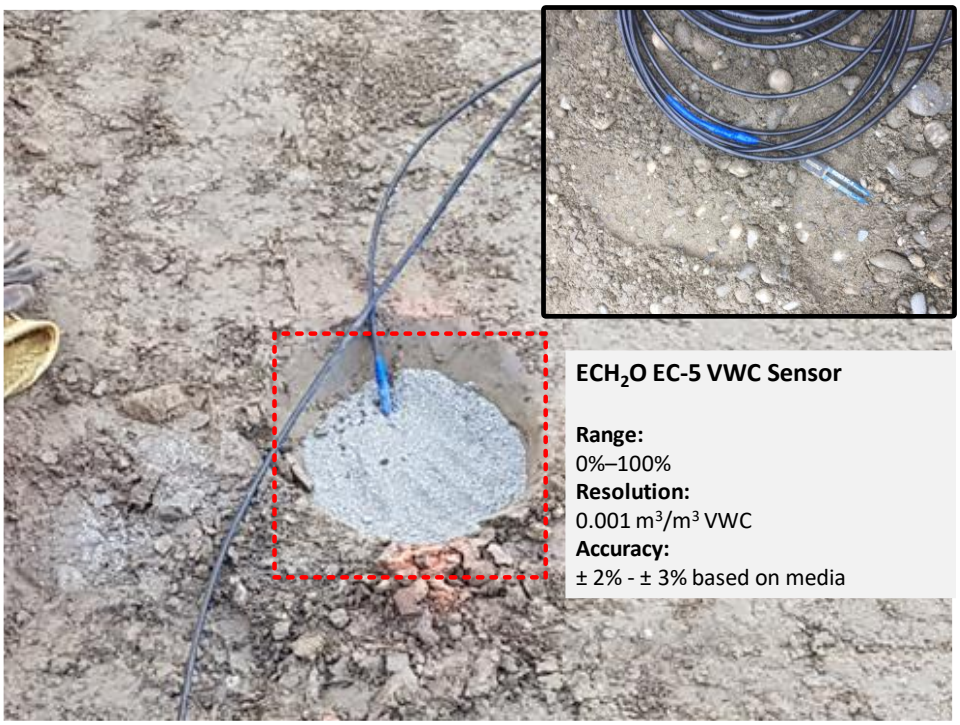

Figure 3.8 Sensor installation

After the first layer of sensors were installed for both Cross Sections 1 and 2, the H2Ri wicking fabric was installed, as shown in Figure 3.9. As mentioned in the test design section, there were several critical aspects requiring special attention. Firstly, the overlapping width of two pieces of the wicking fabrics was 1 ft. Secondly, the wicking fabric at the edge of the roadway should be at the bottom of the wicking fabric installed beneath the main lanes. This requirement allows excess water to flow from the main lanes to the edges. Thirdly, for the wicking fabric installed at the main lanes, the direction of the wicking fiber is parallel to the transverse direction of the road. However, the direction of the wicking fiber is parallel to the longitudinal direction of the road at the edge of the roadway.

Figure 3.9 Installation of H2Ri wicking fabric

After completion of the installment of the H2Ri wicking fabric, a drainage ditch was excavated to direct the excess water to a dry well located on the southeast corner of the test section, as shown in Figure 3.10. The length and depth of the drainage ditch was 20 ft. and 6 ft., respectively. The drainage ditch was leveled to a 10º grade so that the excess water could be directed to the dry well. Then, the subgrade soil was backfilled to the drainage ditch. To direct the surface water to the dry well, a second layer of the H2Ri wicking fabric was installed. One soil moisture sensor was also installed within the backfill subgrade soil to monitor the water content variations within the dry well. Finally, the trench and the dry well were backfilled with Type A fill and compacted to the same grading of the roadway using a vibratory plate compactor.

Figure 3.10 Excavation of drainage ditch

Figure 3.11 Second layer of H2Ri wicking fabric

As for the main lanes of the roadway, the second layer of sensors were installed at Cross Sections 1 and 2 before the Type A fill was placed on site. The sensors were located 2 in. above the H2Ri wicking fabric. After the sensors were installed in place, an intermediate vibrating

compactor was used to compact the Type A fill, as shown in Figure 3.12. Water was spread on the road surface to facilitate the compaction process. The Type A fill was compacted to a thickness of 10 in. and graded to 2 in. below the final road surface grade. Then, the third layer of the sensors was installed. The wiring for the final set of sensors was encased in a flexible steel conduit to protect it from possible damage from the compaction of the finishing layer. The final 2 inches of the roadway were backfilled and compacted with RAP and the final road condition after rehabilitation is shown in Figure 3.13.

Figure 3.12 Compaction of Type A fill

Figure 3.13 Road condition after rehabilitation

For the test section on the east side of the Yukon Drive, the excavation, sensor installation, and backfill procedures were the same as on the west test section. Therefore, the detailed information regarding the construction process will not discussed again. However, according to the test design in Figure 3.3, the drainage design for Cross Section 4 is different compared with that on the west side test section. Therefore, this part mainly focuses on demonstrating the construction process of the drainage ditch on the east test area of the Yukon Drive. After excavation and leveling of the subgrade soils, the drainage trench was excavated on the east edge of the test area, as shown in Figure 3.14. The drainage trench extended to the ground surface 46 ft. away from the southeast corner of the test area.

Figure 3.14 Excavation of drainage trench

Error! Reference source not found. shows the installation of the drainage pipe. The H2Ri wicking fabric was extended to the drainage trench. As shown in **Error! Reference source not found.**(a), diameter of the HDPE pipe was 3 inches and was first placed on top of the wicking fabric. The drainage pipe was cut on one edge so that the extended part of the wicking fabric could be inserted into the pipe. **Error! Reference source not found.**(b) shows the protective woven geotextile that covered the top of the H2Ri wicking fabric to prevent the pipe from clogging and the wicking fabric from being contaminated. Then, the drainage trench was backfilled with Type A fill and compacted using the intermediate vibratory compactor. Figure 3.16 shows the completion of the drainage. As shown in the figure, excess water was observed flowing out of the drainage pipe, indicating that the drainage system functioned as expected.

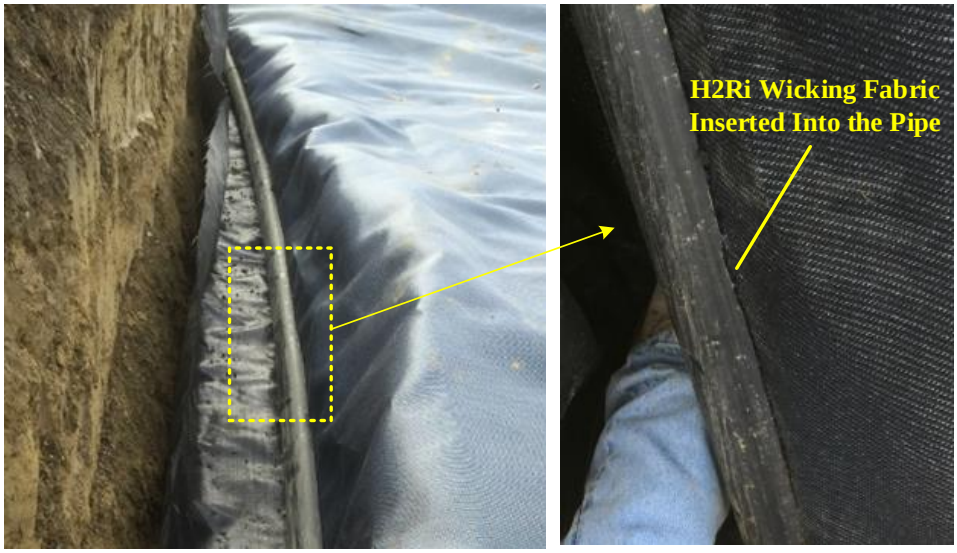

(a) Drainage pipe above the H2Ri wicking fabric

(b) traditional woven geotetxile coverage on top of the pipe

Figure 3.15 Installation of drainage pipe

Figure 3.16 Drainage pipe outlet

3.2 Test Site II: Toklat Way

Introduction of Test Section

Figure 3.17 shows the top view of the second test section, located on the north side of the Reichardt Building. The in-situ soil is a silty soil which is frost susceptible. According to previous observations, frost heave occurred during the winter and a soft spot was reported in early spring each year. Conventional treatments were not effective in dealing with frost heave issues. The purpose of this test section was to evaluate the effectiveness of the H2Ri wicking fabric to mitigate the frost boil issue.

Figure 3.17 Test Section II: Toklat Way

Test Design

The selected test section started at the T-shape intersection and extended 320 ft. to the south, as shown in Figure 3.18. Within the testing area, a 300 ft. out of 320 ft. test section was installed with the H2Ri wicking fabric while the remaining 20 ft. served as a control section without the wicking fabric. Within the treated area, two sections were selected, including Section A (235 ft. from the starting line) and Section B (280 ft. from the starting line).

Figure 3.18 Test section layout at Toklat Way

Figure **3.19** shows the test designs of each cross section. The roadway consisted of three layers, including a 6-inch thick gravelly subbase on top of the subgrade, a 4-inch thick D-1 material as base course, and a 2-inch thick asphalt surface course. For Cross Sections A and B (Figure **3.19** (a) and (b)), the wicking fabric was installed at the bottom of the subbase. As for the control case, Cross Section C (Figure **3.19**(c)), no wicking fabric was installed. In total, three layers of sensors were installed within the subgrade, subbase and base course. For each cross section, there were 5 sensors within the base and subbase layer and were evenly distributed from the west bound to the east bound of the road. As for the subgrade layer, there were 7, 9, and 7 sensors installed for Cross Sections A, B, and C, respectively.

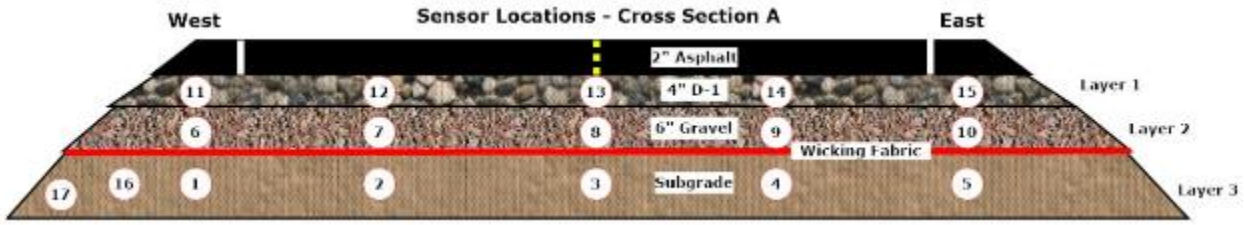

(a) Cross Section A

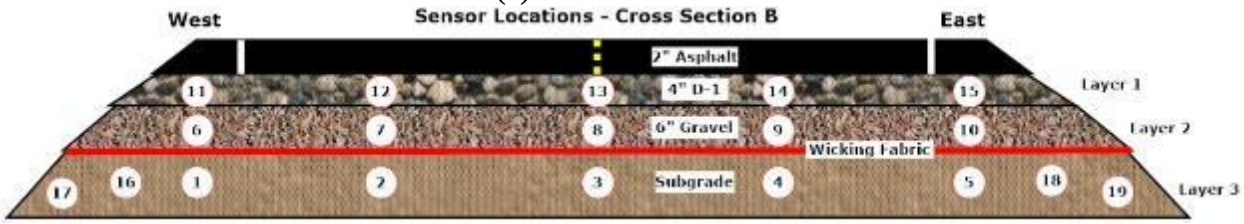

(b) Cross Section B

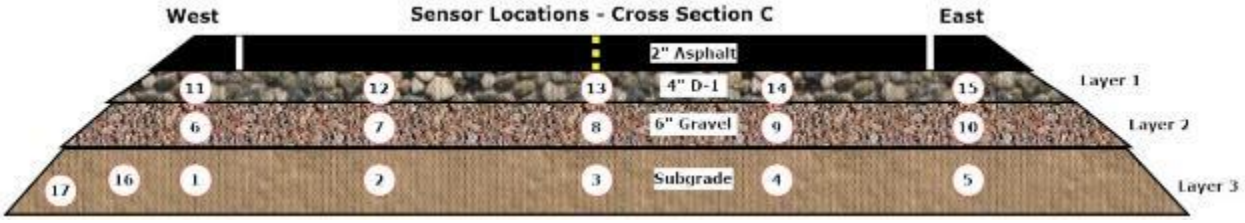

(C) Cross Section C

Figure 3.19 **Test Design of Cross Sections**

Construction Process

According to the original test design, the construction process should have commenced in 2017. However, due to budget limits, the construction was postponed to the summer of 2019. The construction ran from June 29, 2019 to July 1, 2019 and the setup of the data acquisition system was completed on July 22, 2019. It is important to point out that during the excavation process, an unexpected area with a very soft spot was observed on site at the northwest corner of testing area, as shown in Figure 3.20(a). When the construction vehicle drove on the soft spot, immediate settlement of the road embankment was observed and the soil behaved plastically. It was highly possible that the subgrade was already saturated. To prove the assumption, the soft area was excavated to a depth of 4 ft. to fully expose the subgrade layer. As shown in the figure, the subgrade was saturated and could not support the overburden traffic load. The cause of such soft subgrade could be explained as follows. Figure 3.20(b) shows the top view of the test section. In general, the elevation of southwest side was higher than the northeast side. During the spring, when snow started to melt, the melting water should flow from the southwest side to the northeast side. However, the elevation of the road embankment was higher than the subgrade and the road itself served as a water dam impeding the water flow. Therefore, the excess water ponded near the intersection and saturated the road embankment. Since the subgrade soil was frost susceptible and remain saturated in early winter due to sufficient water supply from the ponding water, frost heave was expected to occur during the winter time and ice lenses would develop throughout the winter time. Thus, when the subsequent spring arrived, the ice lenses melted and differential settlement was observed and soft spots were expected. The frost boil problem became worse and worse as the freezing-thawing cycle continued. Figure 3.20(c) further shows the 1-1 profile in Figure 3.20(b). Besides the detrimental effect of the ponding water, berms were observed at the edge of the road surface which might be caused by the repetitive

traffic load and snow plowing in winter times. Such berms formed a U-shaped road surface that would impede water drainage in the summer time. The poor drainage conditions would result in saturating the underlying road structures and accelerate the deterioration of the road embankment. The plowed snow was piled at the road slopes and could not be drained out in the early spring, which aggravated the frost boil problem.

However, without additional funding to authorize the engineering change orders, the contractor decided to follow the original design by directly installing the wicking fabric at the bottom of the excavated subgrade soil, as shown in Figure 3.20(d). It is important to point out that none of the test sections covered this soft spot and the soil moisture content within this part of the road could not be monitored. In addition, the authors argue that such treatment might not be able to mitigate the frost boil problem since the excess water could not be properly drained out of the road embankment. With sufficient water supply and the existence of the same type of frost susceptible soil, frost boil problem might reemerge in the coming year.

(a)

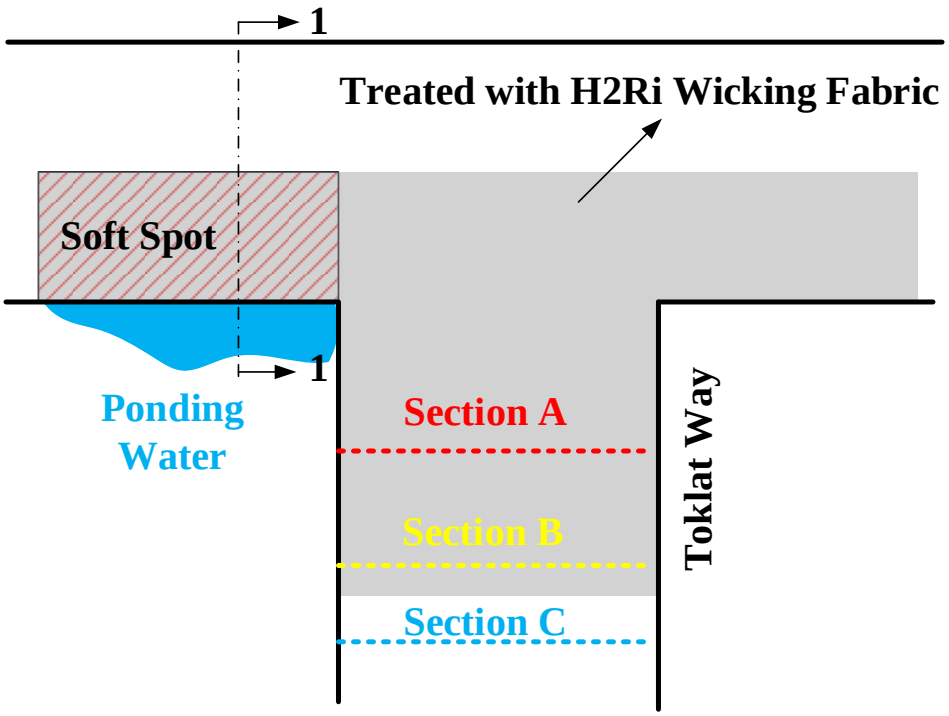
1
Treated with H2Ri Wicking Fabric
Soft Spot
1
Ponding
Water
Section A
Section B
Section C
Toklat Way

(b)

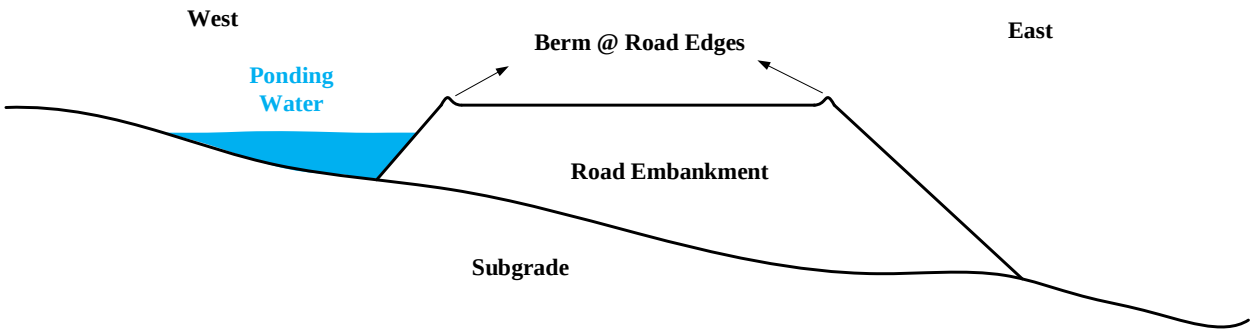
West
Berm @ Road Edges
East
Ponding
Water
Road Embankment
Subgrade

(c)

(d)

Figure 3.20 Unexpected soft subgrade on site

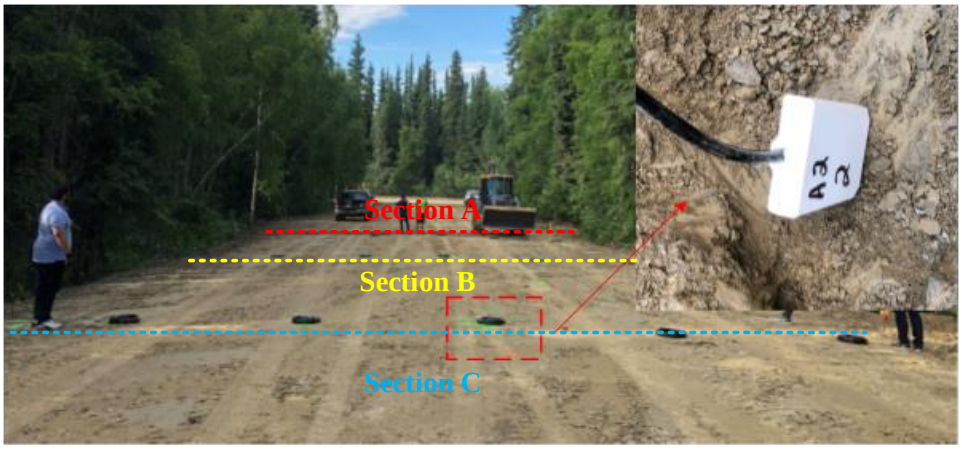

Figure 3.21 Installation of the 3rd layer of sensors

After the surface of the subgrade was cleared and leveled, the locations of the test sections were determined, as shown in Figure 3.21. Cross Section A, B, and C were determined as the red, yellow and blue lines. The 3rd layer of sensors were installed. Since the subgrade soil was a silty soil which was relatively uniform, the probes of the sensors were directly inserted

into the in-situ subgrade. Then, the wires of the sensors were covered with protective conduit, bundled together, and directed to the location of the data acquisition system.

Figure 3.22 shows the installation process of the H2Ri wicking fabric. The length of the roadway was much wider than the roll length and three rolls of the wicking fabric were used. It is important to point out that the two rolls at the road edges must be installed prior to the middle one. This requirement facilitated the water draining from the center of the road to the edges and effectively preventing water flowing reversely into the road embankment during heavy rainfalls. In addition, a minimum of 1 foot of overlap was required at the contact area between two adjacent rolls.

Figure 3.22 Installation of the wicking fabric

Figure 3.23 Installation of the 2nd layer of sensors

Figure 3.23 shows the installation of the 2nd layer of sensors. This layer of sensors was installed within the subbase layer that is a gravelly material. To ensure the consistency of sensor readings in gravelly material, uniform sand was used as a media. A 2 inch hole was first made and the sensor was put horizontally into the hole with the probes inserting into the sand layer. After that, the hole was backfilled with the subbase material and loosely compacted by hand. After the second layer of sensors were installed, the base course material was shipped on site and compacted with an intermediate roller, as shown in Figure 3.24(a). During the compaction process, water was continuously spread on the road and the surface of the base layer was graded with a 2º grading in the transverse direction, as shown in Figure 3.24(b). Finally, the 2-inch asphalt surface course was paved on July 1, 2019 and Figure 3.25 shows the road surface condition after the completion of rehabilitation.

(a)

(b)

Figure 3.24 Base course compaction and grading

Figure 3.25 Road condition after rehabilitation

CHAPTER 4: PRELIMINARY TEST RESULTS

This chapter covers the data collected from Test Section I, Geogerson Botanical Garden. The construction of Test Section II, Toklat Way, was completed in early July, 2019 and insufficient data has been collected to perform the analysis.

Error! Reference source not found. shows the climatic data at Test Section I. The maximum precipitation was 1.1 inches and occurred on October 27, 2018. In general, the frequencies of precipitation were higher from August to October as compared to other months. Note that the rainfall was observed on December 7, 8, and 13, 2018. Even though the average temperature on those days were below 0 ºC, the maximum temperature was all above 0 ºC, indicating that rainfalls occurred during the daytime. **Error! Reference source not found.**(b) shows the daily maximum, minimum, and average temperatures from October 2017 to November 2018. The average daily temperature dropped below 0 ºC in late October, 2017 and rose above 0 ºC in late April, 2018.

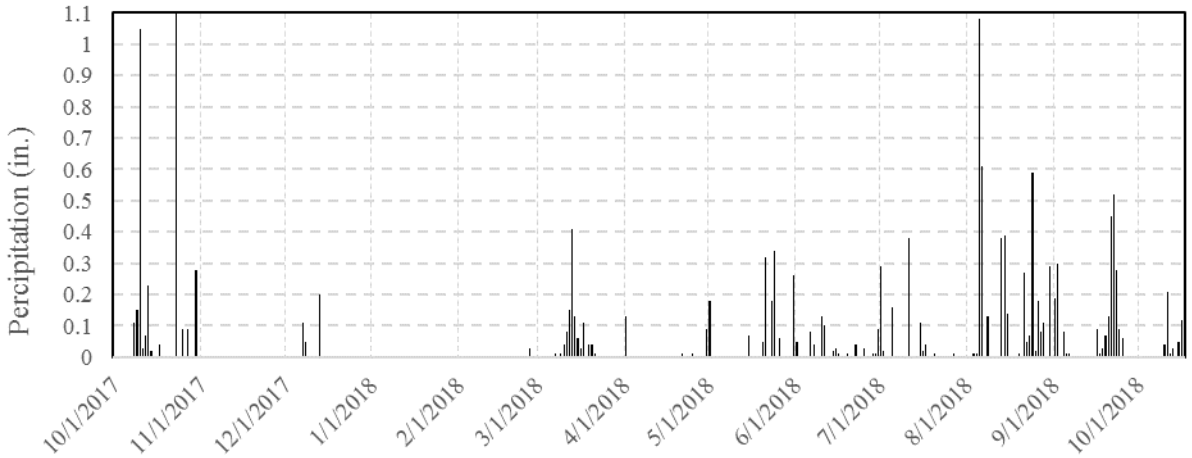

(a) Daily precipitation data

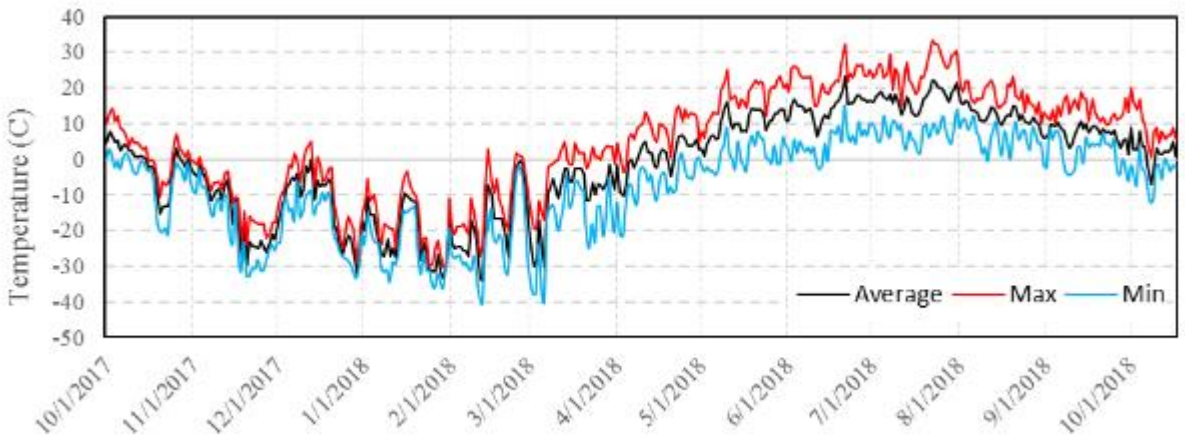

(b) Daily temperature data

Figure 4.1 Climatic Data

Among all the sensors, several soil volumetric water content (VWC) readings were not consistent because part of the volumetric readings were either negative values (lower than the minimum value of 0.0) or greater than the highest value of 1.0. However, temperature readings from those sensors were consistent. In total, 13 VWC sensors were deemed to be damaged. In section 1, sensors 3 and 10 were damaged. In section 2, sensors 5, 6, 8, 9, 13, 14, and 15 were damaged. In section 3, sensors 2, 9, and 14 were damaged. In section 4, only sensor 9 was damaged. As for the temperature readings, only sensor 7 in section 4 was not consistent. In many cases, most of the sensors show the same pattern in measuring volumetric water content. Here representative data is presented and discussed, and the raw data regarding each sensor is presented in the APPENDIX. In addition, the notation in the following figures are defined as follows. The number after the "S" letter represents section number and the second number represents the sensor number in that section. The sensor locations were shown in Figure 3.3. It should also be noted that some sensors at some points show unrealistic values. For instance, sensor S1 1 (sensor 1 in section 1) shows a few negative values and sensor S1 14 (sensor 14 in section 1) shows several values larger than 1. Neglecting these unrealistic values leads to following results and discussion.

Error! Reference source not found. shows the volumetric water content variations at sensors 10, 11, and 12 in section 4. S4 10 was the closest sensor to the road surface. S4 11 was below S4 10 and S4 12 was the deepest sensor. These sensors were about 8 - 10 feet to the east of the section 4 centerline and on the downside of the roads cross section grading. the VWC in these sensors dropped significantly in October and November 2017. By looking at the sensors' temperature readings, shown in Figure 4.3, the sharp decrease in VWC reflects the moment when the temperature dropped below 0 ˚C. The temperature at the deepest sensor dropped below 0 ˚C approximately 22 and 20 days after the same phenomenon happened at sensor S4 10 and S4 11 respectively. Since the vertical distance of S4 11 and S4 12 were closer than that of S4 10 and S4 11, it implies that most of the time lag in reaching below the freezing temperature was caused by water's large latent heat of fusion. Based on the sensors' readings, the soil below the wicking fabric had a higher water content and it required a lot of energy decrease the temperature of the underlying soil. The freezing period lasted until mid-March 2018. During this period, although there were several precipitations events, the VWC didn't change, indicating that these precipitations were either in form of snow or, rain that froze before percolating under the road surface.

In early spring of 2018, a sharp increment in VWC was observed due to the thawing season and this phenomenon was an indication of the commencement of the melting season. The highest VWC increment was observed in sensor S4 12, increasing from 9% to 42%. S4 12 remained at its peak VWC and lasted for weeks from the beginning of the thawing season. In contrast, the sensors S4 10 and S4 11, located above the wicking fabric, showed a sharp decrement after reaching their peak VWC values. During the thawing season, the excess water percolated downward under the influence of gravity. When the waterfront reached the location of

the wicking fabric, part of the water was laterally drained to the edge of the roadway and the rest continued to percolate to the underlying soil. Since the permeability of the underlying soil was significantly lower than the base course, water ponded in the hole were the sensor was installed. In addition, the sharp increase in VWC during the summer time was related to the amount of precipitation. By comparing the precipitation data presented in Figure 4.1(a) and the VWC readings, nearly all of the sharp increments in VWC were related to rainfall events. S4 10 and S4 11 showed various increments with small amplitude while such phenomenon were not observed for S4 12. This indicates that the wicking fabric could effectively drain all the excess water out of the road embankment during lighter rainfalls.

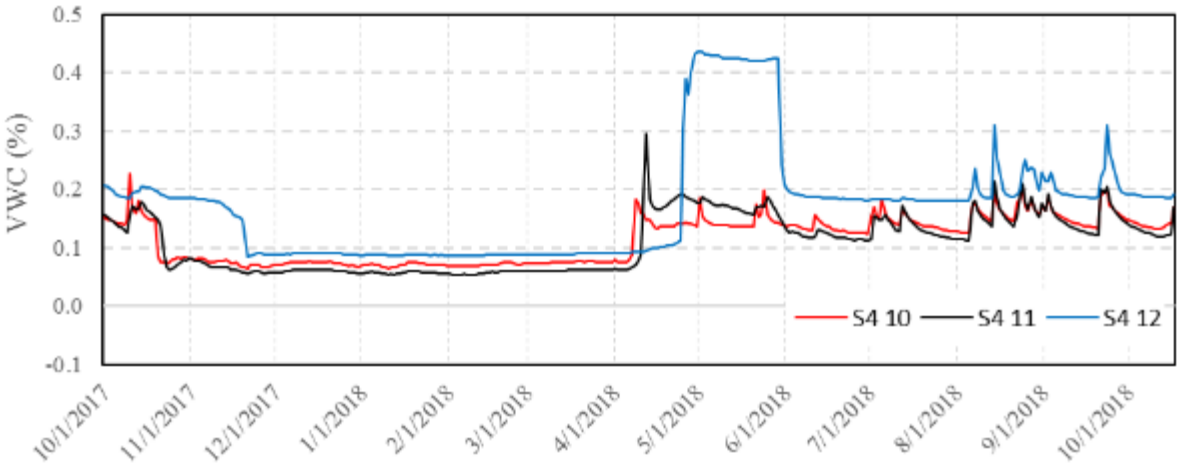

Figure 4.2 VWC at sensors 10 through 12 in section 4

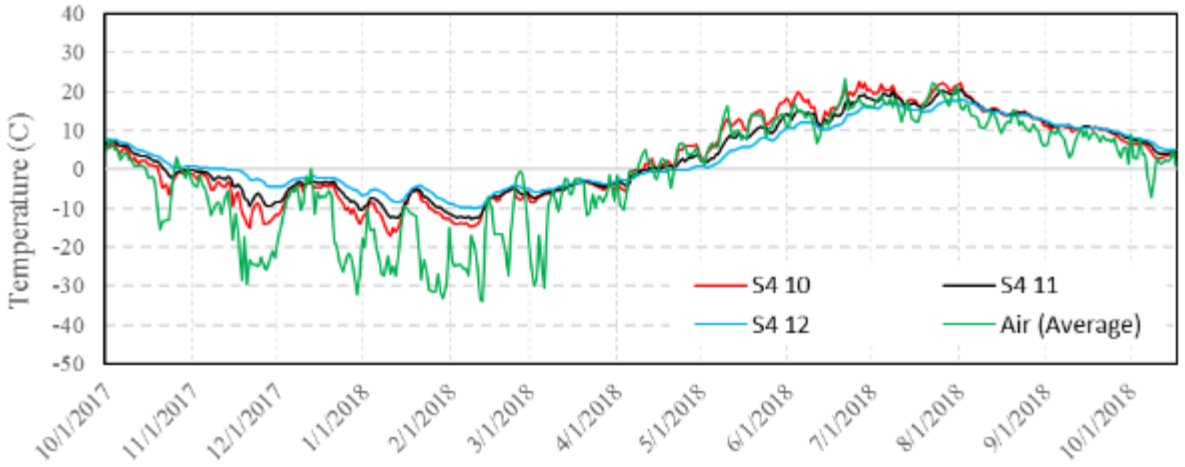

Figure 4.3 Daily temperature at sensors 10 through 12 in section 4

Figure 4.4 0shows the VWC variations of the three sensors that were below the road surface in Section 3. As was discussed before, this is the control section where no wicking fabric was used below the base course material. In contrast to section 4, the soil volumetric water content distribution in the vertical direction was more uniform. In addition, the timespan for the sensors remaining at the peak values was significantly longer in section 3 than in section 4 during the thawing season staring in May 2018. This fact indicates that the wicking fabric worked efficiently to drain the excess water out of the road embankment.

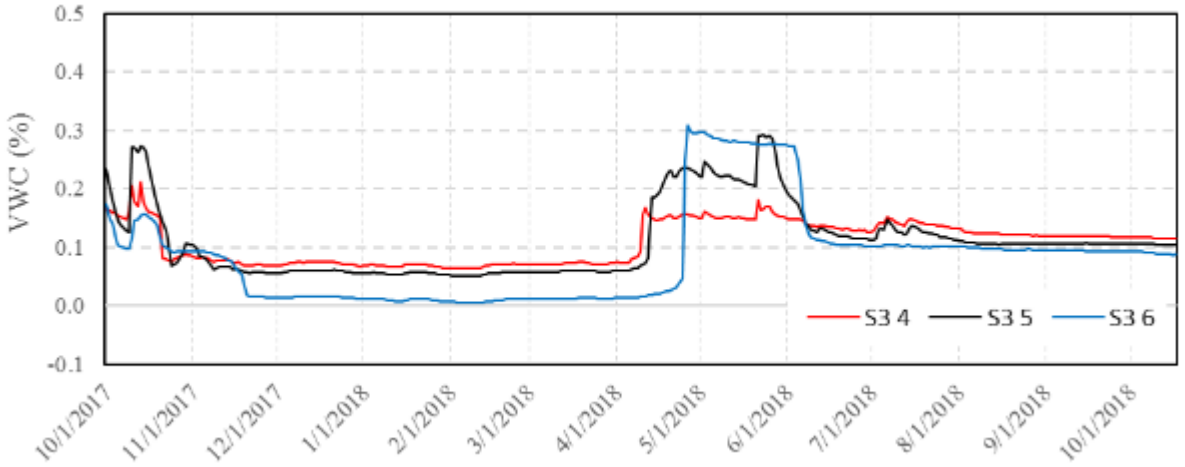

Figure 4.4 VWC at sensors 4 through 6 in section 3 (control section)

To further demonstrate the moisture migrations within each test section, the raw data for each sensor was used to generate soil volumetric water content and soil temperature contours. Figure 4.5 Figure 4.6 show the VWC and temperature variations in each test section on February 1, 2018. This day was selected because it was in the middle of the freezing period. In the temperature contours, the freezing front was below the location of the deepest sensors and all the base course material was frozen. Consistent observations were observed in the VWC contours in which the VWC values were lower than 8% in each test section. However, VWC values near the location of the H2Ri wicking fabric were significantly lower than the rest area and the average VWC value was approximately 2% in sections 1, 2, and 4. In contrast, the average VWC was 5% in section 3 where no H2Ri wicking fabric was installed.

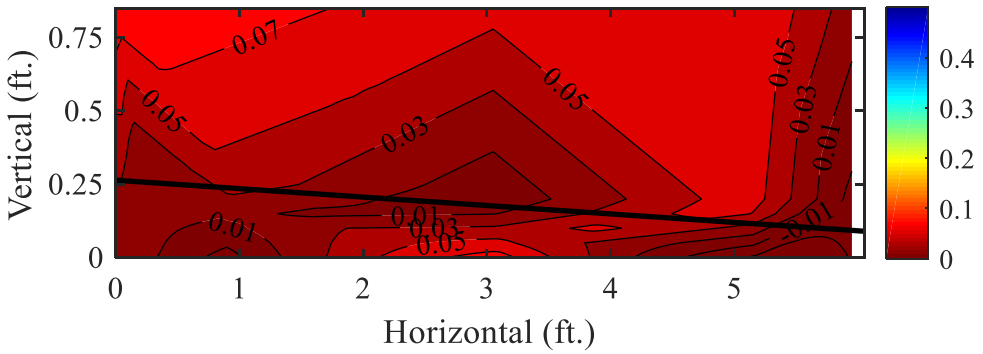

(a) VWC distribution at Section 1

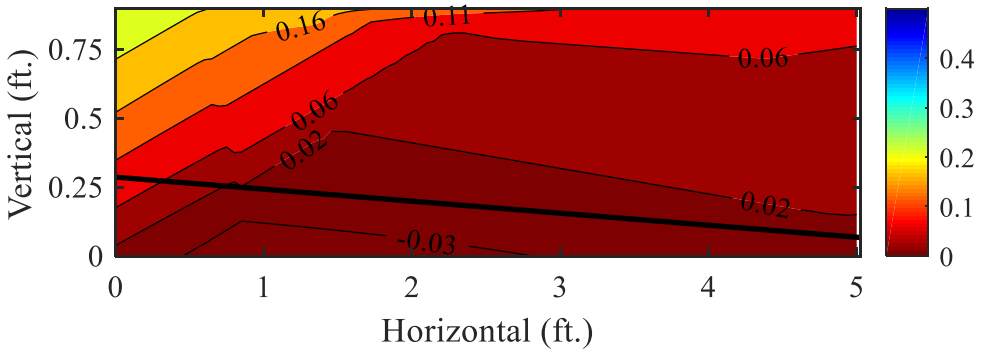

(b) VWC distribution at Section 2

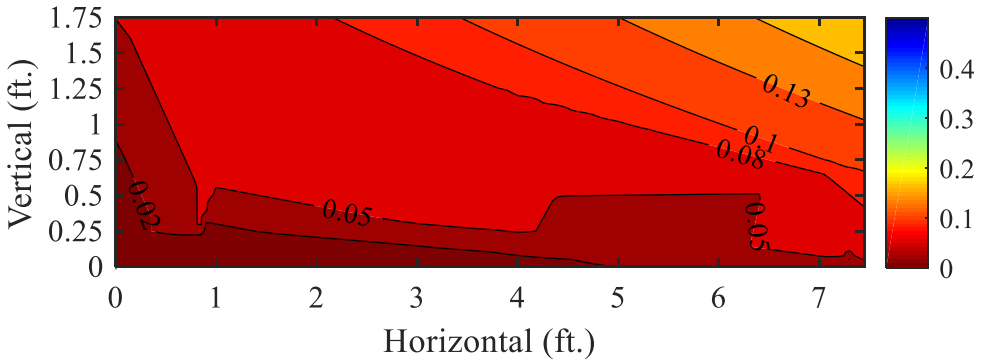

(c) VWC distribution at Section 3

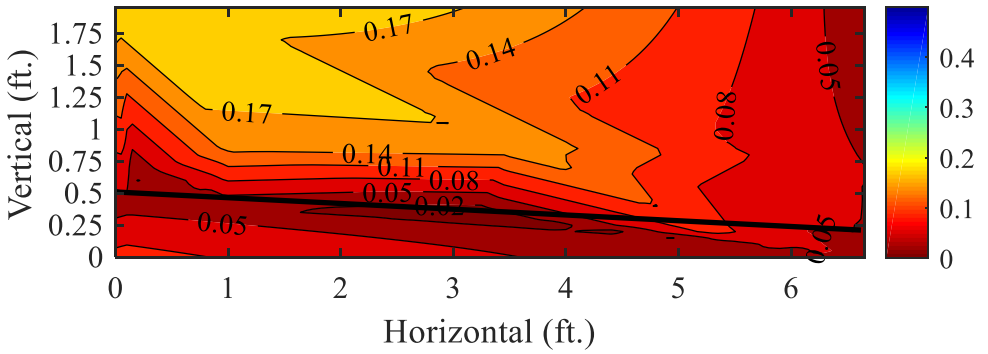

(d) VWC distribution at Section 4

Figure 4.5 VWC at different sections during thawing on February 1, 2018 at noon

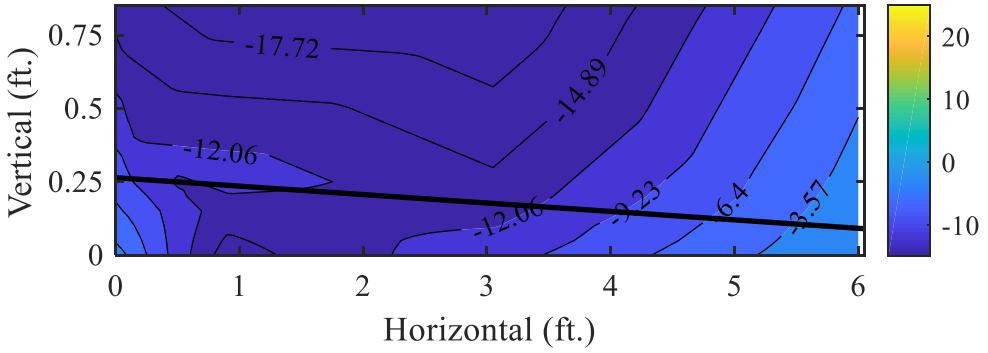

(a) Temperature distribution at Section 1

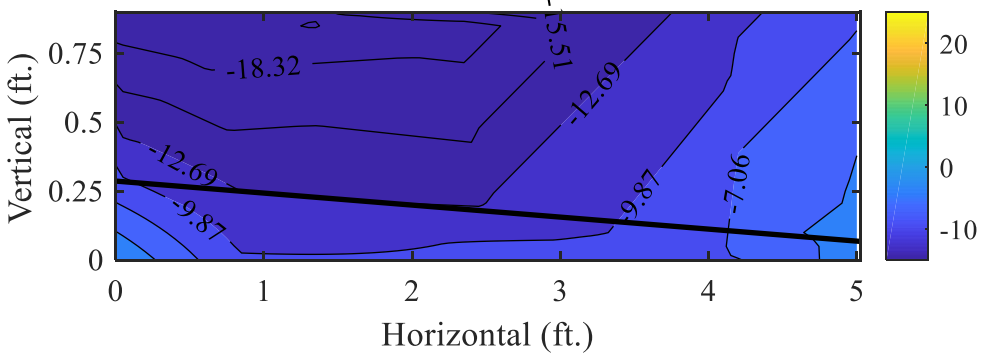

(b) Temperature distribution at Section 2

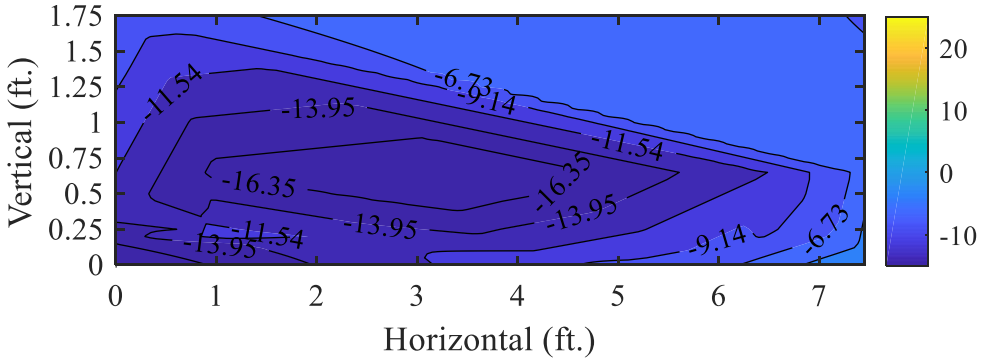

(c) Temperature distribution at Section 3

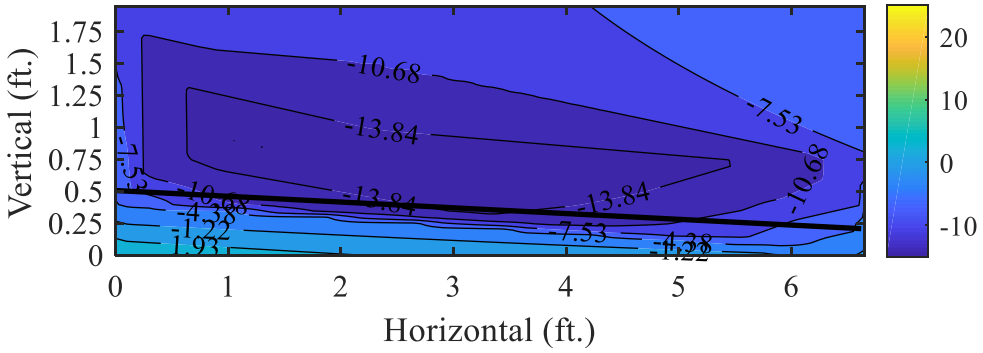

(d) Temperature distribution at Section 4

Figure 4.6 Temperature at different sections during thawing on February 1, 2018 at noon

Figure 4.7 shows the volumetric water content contours in each section on May 5th, 2018. This moment occurred during the middle of the thawing season and the average air temperature was 10 ˚C. In each section, the sensors of the 3rd layer, which were installed within the subgrade soil, showed the peak values. In comparison, the VWC values in the 1st layer, underlying the RAP layer, reached average values of 0.17 in section 1 and section 2, 0.1 in section 3, and 0.26 in section 4, respectively. The VWC distribution in the vertical direction was more uniform in section 3 but with the lowest magnitude. However, an obvious VWC difference was observed between the locations at the wicking fabric and above it in section 4. Figure 4.8 shows that the the temperature values were all above 0˚C, indicating that the entire road embankment was unfrozen at this moment of the year.

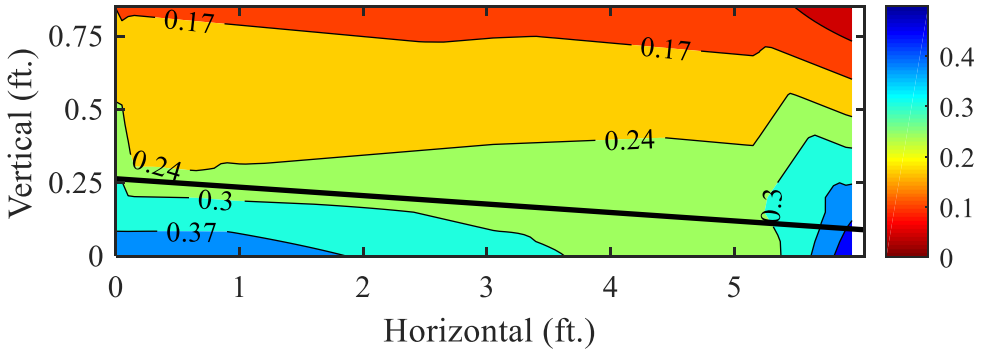

(a) VWC distribution at Section 1

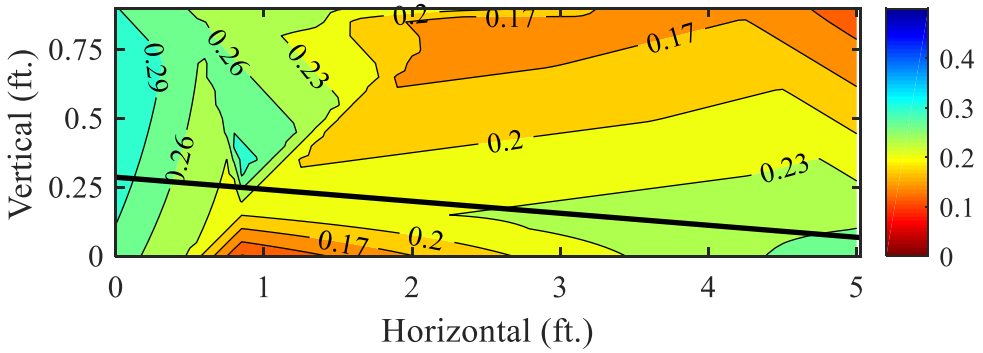

(b) VWC distribution at Section 2

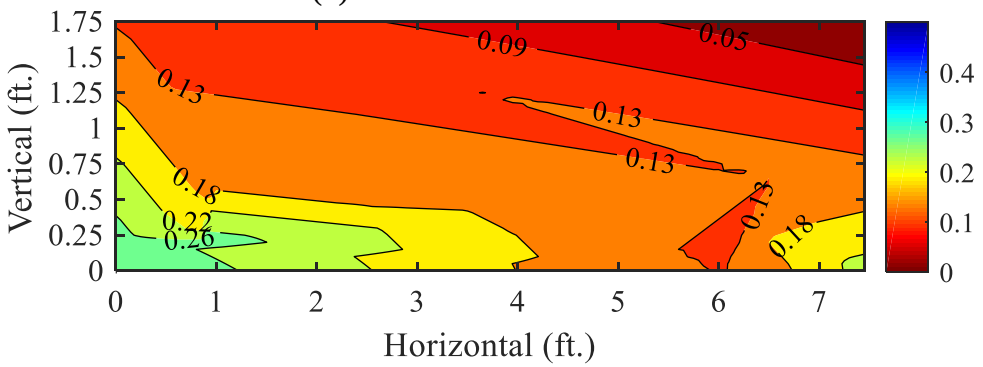

(c) VWC distribution at Section 3

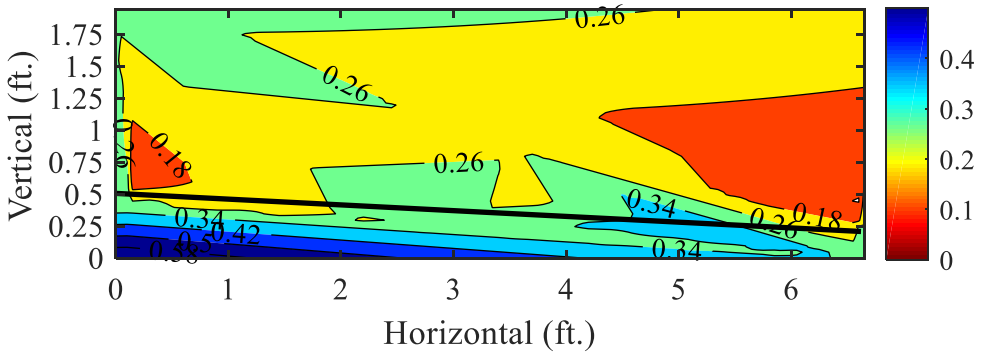

(d) VWC distribution at Section 4

Figure 4.7 VWC at different sections during thawing on May 15, 2018, at noon

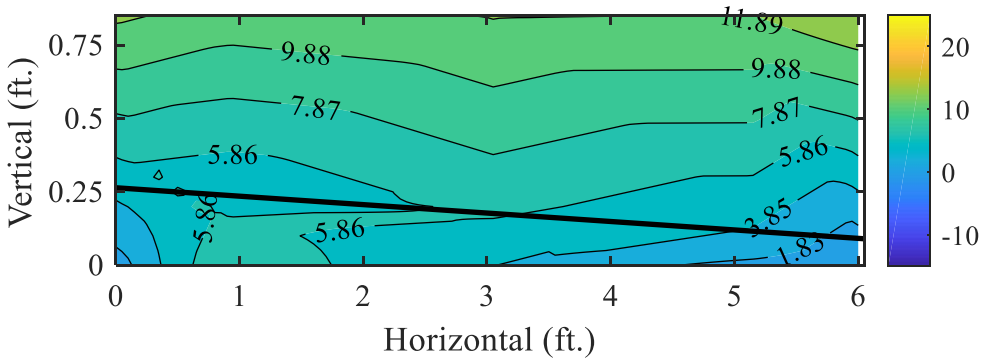

(a) Temperature distribution at Section 1

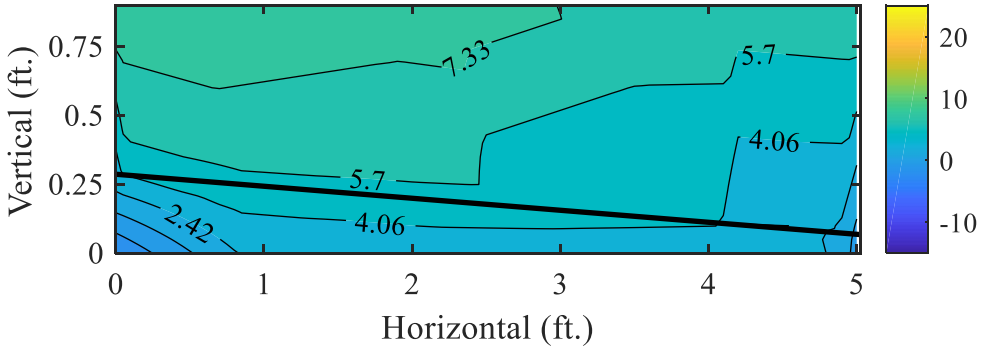

(b) Temperature distribution at Section 2

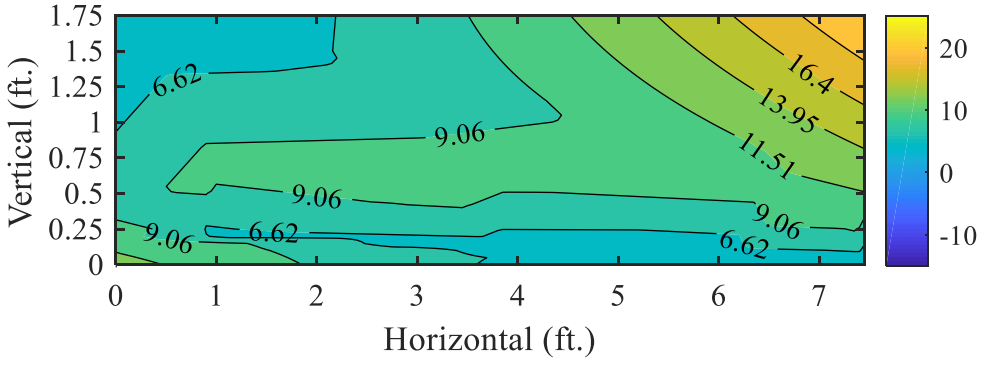

(c) Temperature distribution at Section 3

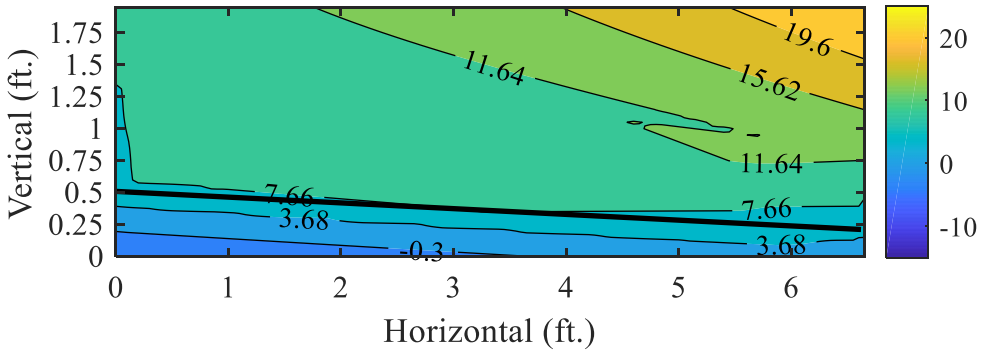

(d) Temperature distribution at Section 4

Figure 4.8 Temperature at different sections during thawing on May 15, 2018, at noon

After the thawing season has passed and all the melting water drained out of the road embankment, the VWC dropped to a lower value and kept constant until the next precipitation occurred. In order to compare the sensor readings at the end of the thawing season, the VWC and temperature contours were provided in each test section on June 20, 2018, as shown in Figure 4.9Figure 4.10. The figures explicitly showed the effectiveness of H2Ri in the reduction of water content. In section 1, the VWC value right beneath the RAP layer dropped from 0.17 on May 15 to 0.14 on June 20. In section 2 for the same period at the same location the VWC dropped from 0.17 to 0.13 and the value dropped from 0.26 to 0.23 in section 4. However, in section 3 where there is no wicking fabric, VWC increased over the same period. This fact indicates that the H2Ri wicking fabric was effective and efficient in draining the excess water out of the road embankment. The soil strength was expected to increase with time and with the soil water content lower than the saturation values, the frost boil issue was expected to be mitigated.

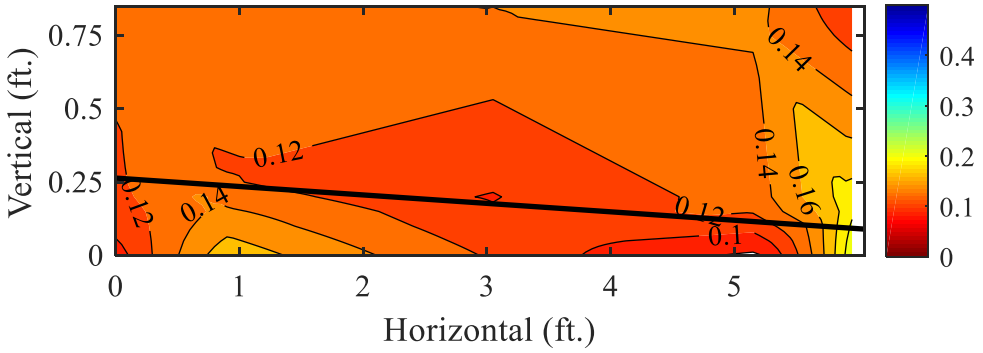

(a) VWC distribution at Section 1

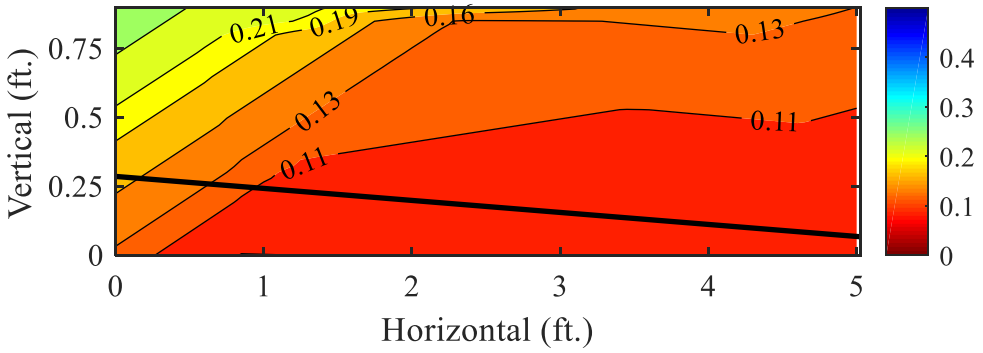

(b) VWC distribution at Section 2

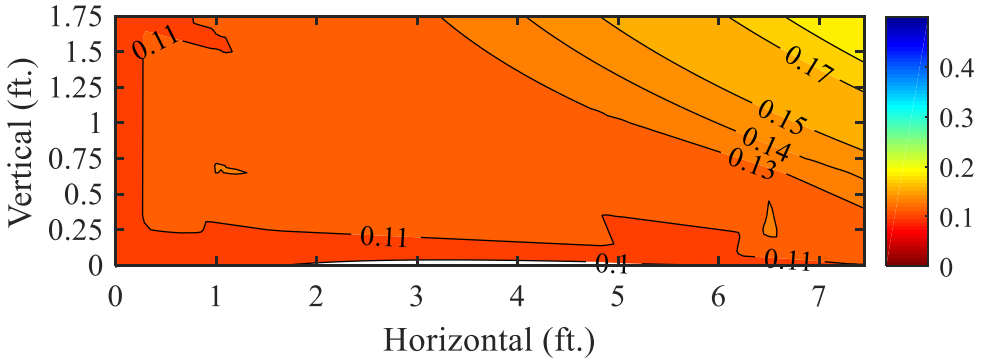

(c) VWC distribution at Section 3

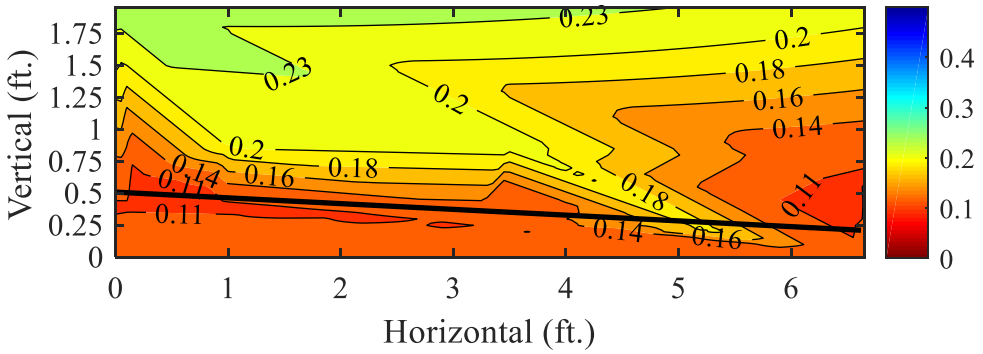

(d) VWC distribution at Section 4

Figure 4.9 VWC at different sections during thawing on June 20, 2018, at noon

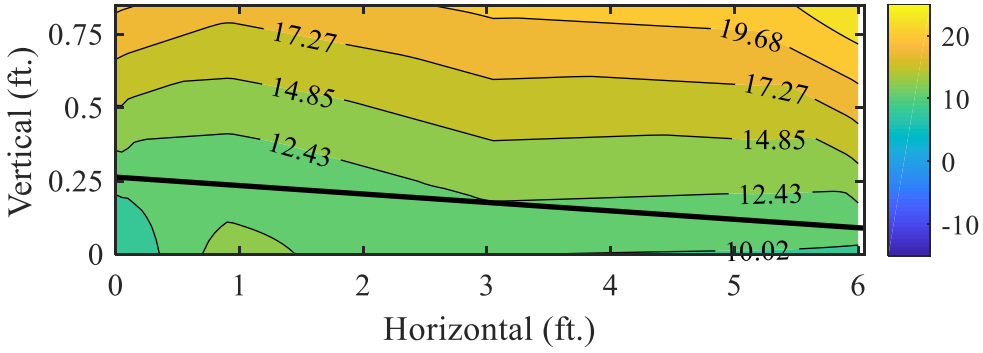

(a) Temperature distribution at Section 1

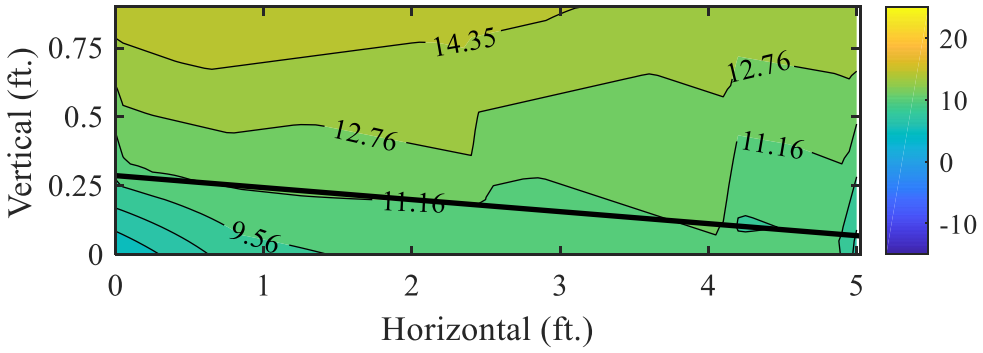

(b) Temperature distribution at Section 2

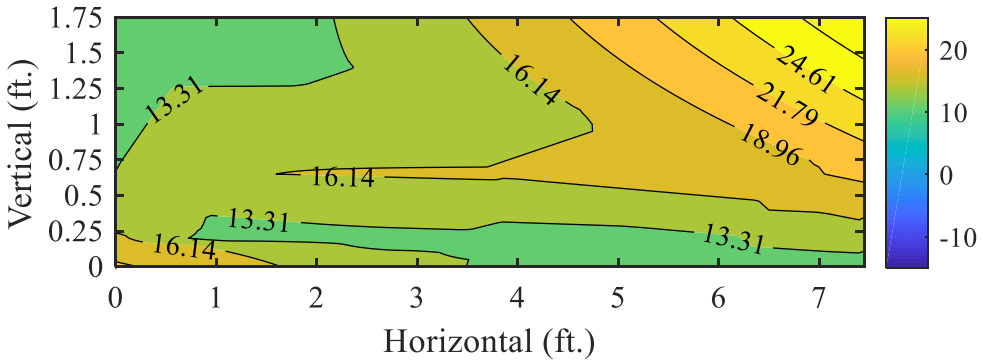

(c) Temperature distribution at Section 3

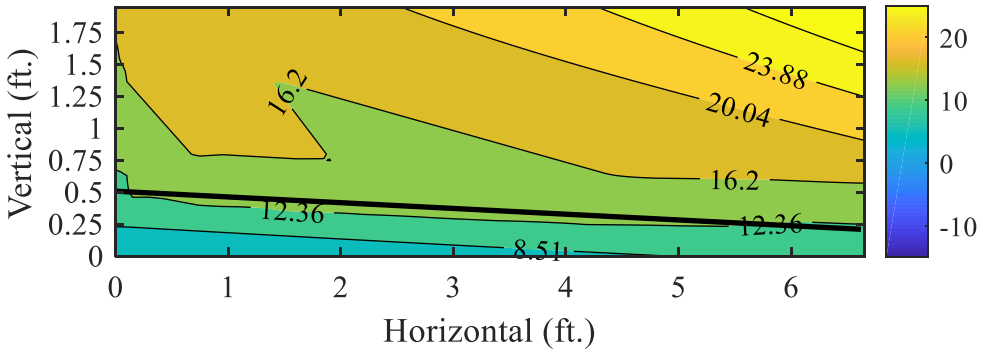

(d) Temperature distribution at Section 4

Figure 4.10 Temperature at different sections during thawing on June 20, 2018, at noon

CHAPTER 5: CONCLUSIONS

To verify the effectiveness of the bio-wicking system to mitigate the frost boil issue, two test sections (paved and unpaved roadways) with low volume roadway were selected. The full depth rehabilitation at each test section was performed and the H2Ri wicking fabric was installed at the top of the subgrade layer. Soil moisture and temperature sensors were installed to monitor the moisture migration within the road embankments. The major findings of the project are as follows:

- For Test Section I at the Botanical Garden, the monitoring results indicate that the wicking fabric was effective in reducing the soil water content. The controlled section showed a higher water content value in the summer time. In contrast, the water content values at the other three sections showed lower values.

- The melting of snow caused significant increase in soil water content and it could take up to two months to drain the excess water. During this period, the water content of the base course above H2Ri wicking fabric quickly decreased, indicating that the H2Ri wicking fabric was effective and efficient in draining the excess water out of the road embankment. In contrast, the drainage of excess water was much slower in section 3 where no H2Ri wicking fabric was installed.

- However, the sections selected in Test Section II at the Toklat Way did not cover the soft spot observed during the construction process. Since no additional funding could support a change in the engineering design, the excess water was expected to be ponded near the road embankment and soft spots might not be effectively mitigated. In addition, the construction of the test section completed in July 2019 and insufficient data could be

collected to perform the analysis. A longer monitoring period of time is required before any conclusive information could be provided.

REFERENCES

Carlson, L. E. and Nixon, J. F. (Derick) (1988) "Subsoil investigation of ice lensing at the Calgary, Canada, frost heave test facility," *Canadian Geotechnical Journal*. NRC Research Press Ottawa, Canada , 25(2), pp. 307–319. doi: 10.1139/t88-033.

Cedergren, H. (1994) "America's Pavements: World's Longest Bathtubs," *Civil Engineering*, 64(9), pp. 56–58. doi: 10.1016/j.bbrc.2005.05.181.

Christopher, B. R. (Barry R. *et al.* (1997) *Pavement subsurface drainage systems*, *NCHRP Synthesis of Highway Practice*. National Academy Press.

DOT&PF (2004) "Alaska Department of Transportation and Public Facilities Standard Specification for Highway Construction."

Esch, D. C. (1995) "Long-term evaluations of insulated roads and airfields in Alaska," *Transportation research record*, (1481).

Google Inc. (2011) "Google Earth," *7.1.2.2041*. doi: 10.1364/OE.9.000567.

Gray, D. H., Tons, E. and Thiruvengadam, T. R. (1994) "Performance evaluation of a cement-stabilized fly ash base," *Transportation research record*, (1440).

Henry, K. (1996) "Geotextiles to Mitigate Frost Effects in Soils: A Critical Review," *Transportation Research Record: Journal of the Transportation Research Board*. Transportation Research Board of the National Academies , 1534, pp. 5–11. doi: 10.3141/1534-02.

Henry, K. S. (1990) *Laboratory investigation of the use of geotextiles to mitigate frost heave*. COLD REGIONS RESEARCH AND ENGINEERING LAB HANOVER NH.

Henry, K. S. and Holtz, R. D. (2001) "Geocomposite capillary barriers to reduce frost heave in soils," *Canadian Geotechnical Journal*, 38(4), pp. 678–694. doi: 10.1139/t01-010.

Lai, Y., Zhang, S. and Yu, W. (2012) "A new structure to control frost boiling and frost heave of embankments in cold regions," *Cold Regions Science and Technology*. Elsevier, 79–80,

pp. 53–66. doi: 10.1016/J.COLDREGIONS.2012.04.002.

Zhang, X. and Presler, W. (2012) “Use of H2Ri Wicking Fabric to Prevent Frost Boils in the Dalton Highway Beaver Slide Area, Alaska.” Alaska University Transportation Center, Alaska Department of Transportation and Public Facilities.

Zhang, Y., Johnson, A. E. and White, D. J. (2016) “Laboratory freeze–thaw assessment of cement, fly ash, and fiber stabilized pavement foundation materials,” *Cold Regions Science and Technology*. Elsevier, 122, pp. 50–57. doi: 10.1016/J.COLDREGIONS.2015.11.005.

Lin, C., Presler, W., Zhang, X., Jones, D. & Odgers, B. 2017. Long-Term Performance of Wicking Fabric in Alaskan Pavements. Journal of Performance of Constructed Facilities, 31, D4016005.

Lin, C. & Zhang, X. 2016. A Bio-Wicking System To Mitigate Capillary Water in Base Course. Center For Environmentally Sustainable Transportation in Cold Climates (Cesticc).

Zhang, X. & Belmont, N. 2012. Use Of Wicking Fabric to Help Prevent Differential Settlements in Expansive Soil Embankments. Geo-Frontiers Congress 2011.

Zhang, X., Presler, W., Li, L., Jones, D. & Odgers, B. 2014. Use of Wicking Fabric to Help Prevent Frost Boils in Alaskan Pavements. Journal of Materials in Civil Engineering, 26, 728-740.

APPENDIX RAW DATA

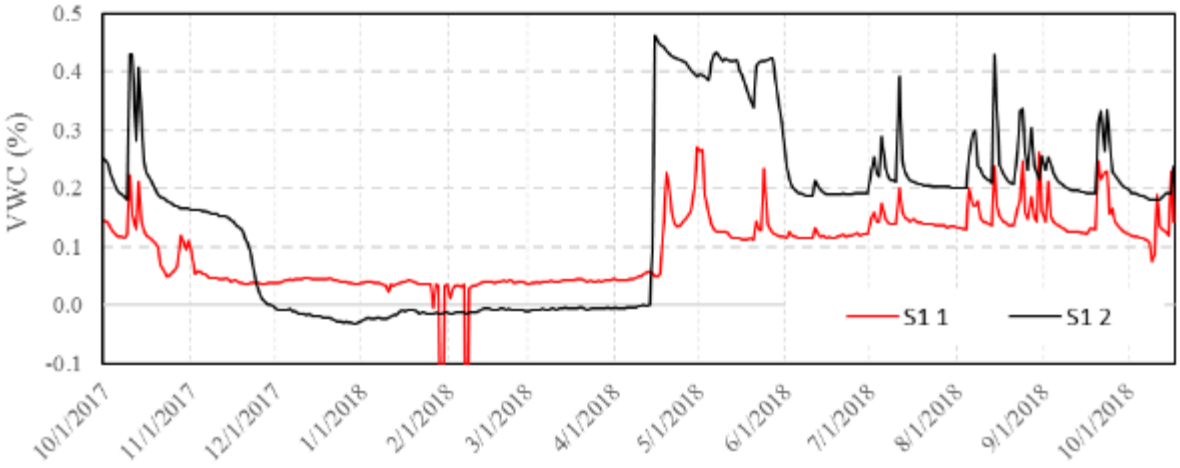

Figure A. 1 VWC at sensors 1 and 2 in section 1

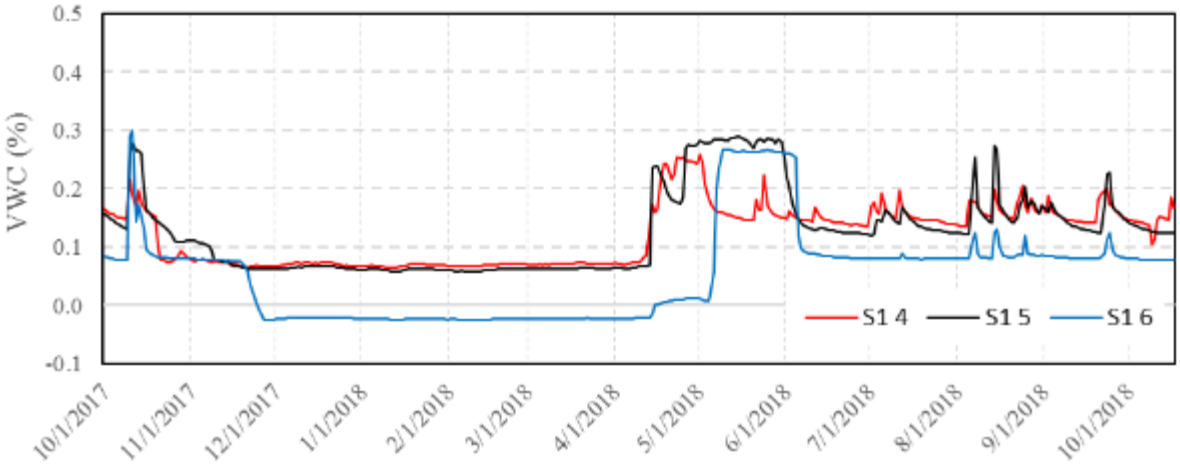

Figure A. 2 VWC at sensors 4 through 6 in section 1

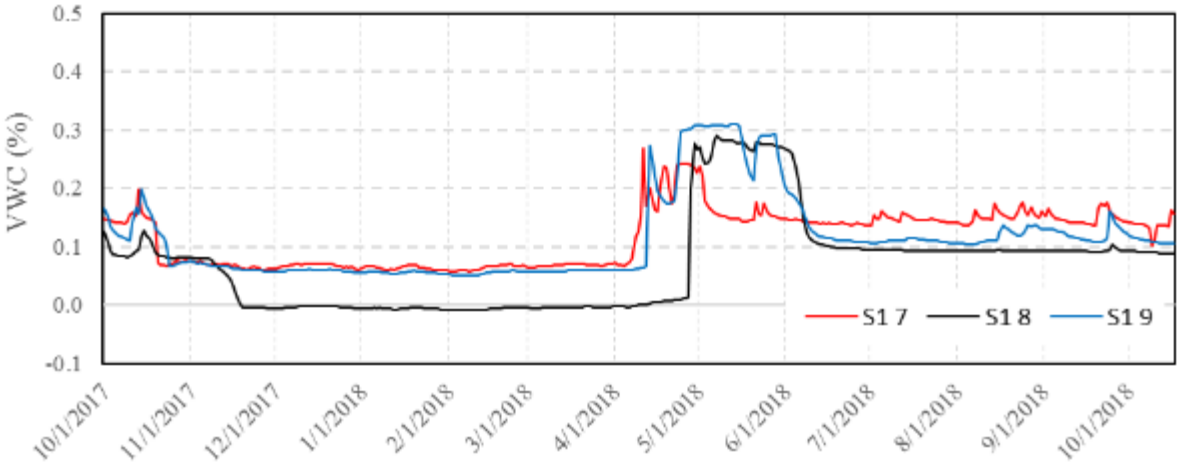

Figure A. 3 VWC at sensors 7 through 9 in section 1

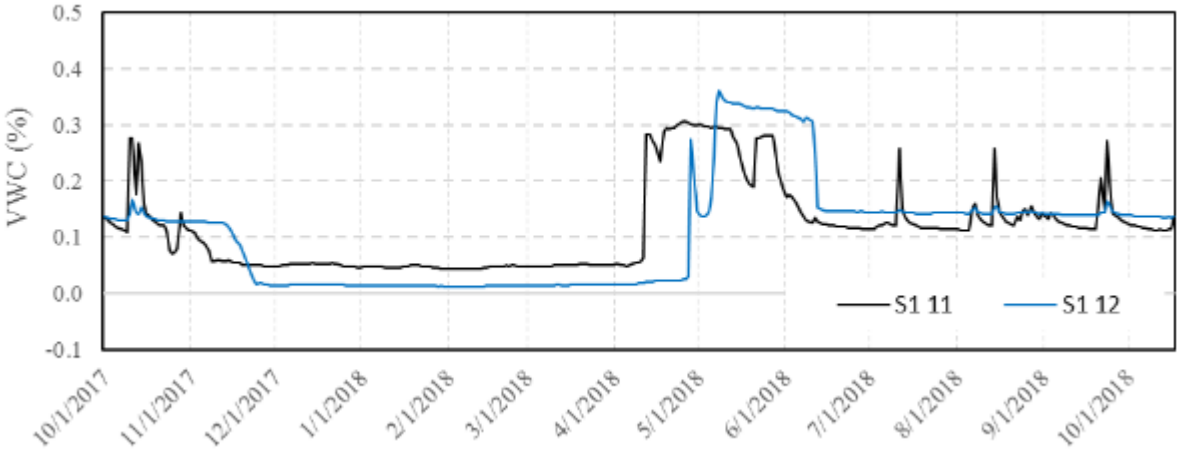

Figure A. 4 VWC at sensors 11 and 12 in section 1

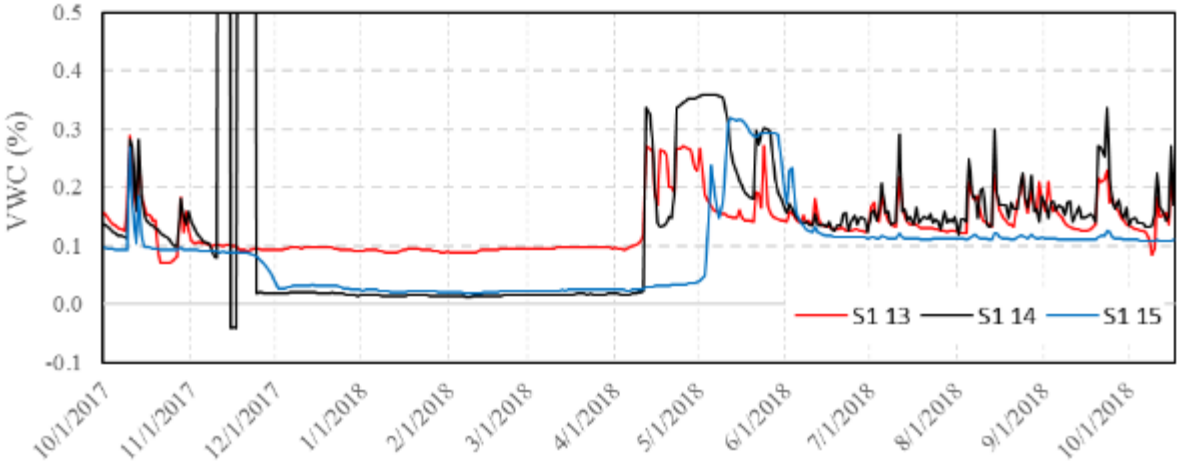

Figure A. 5 VWC at sensors 13 through 15 in section 1

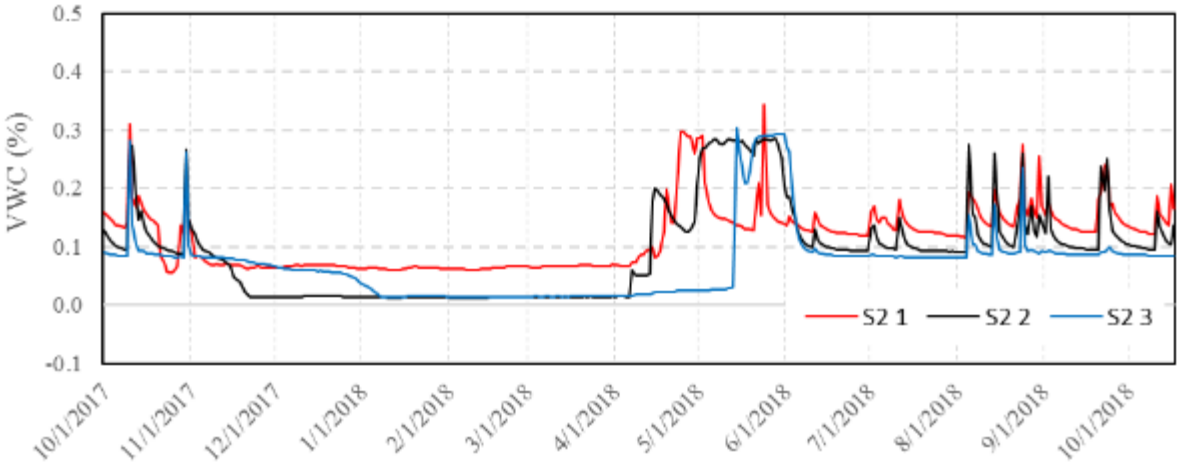

Figure A. 6 VWC at sensors 1 through 3 in section 2

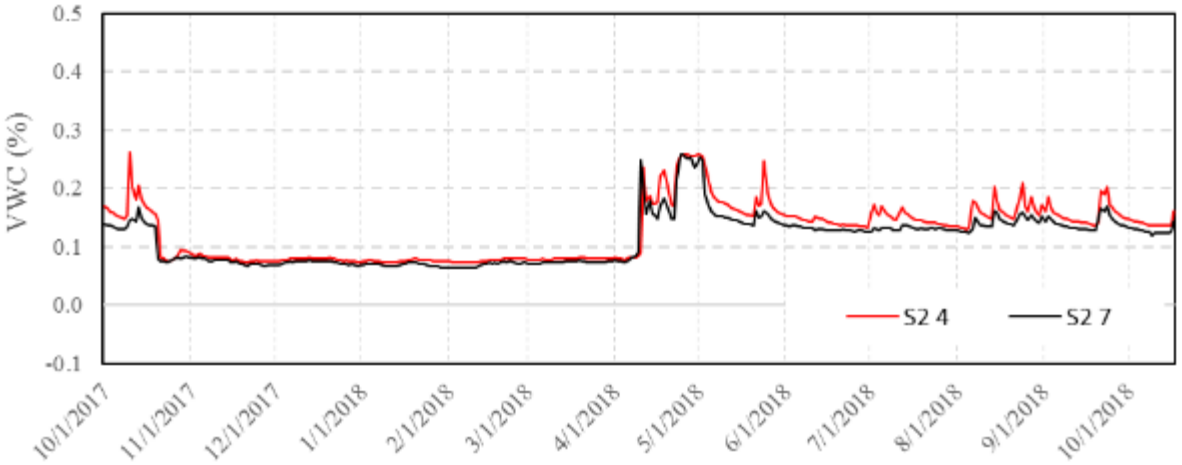

Figure A. 7 VWC at sensors 4 and 7 in section 2

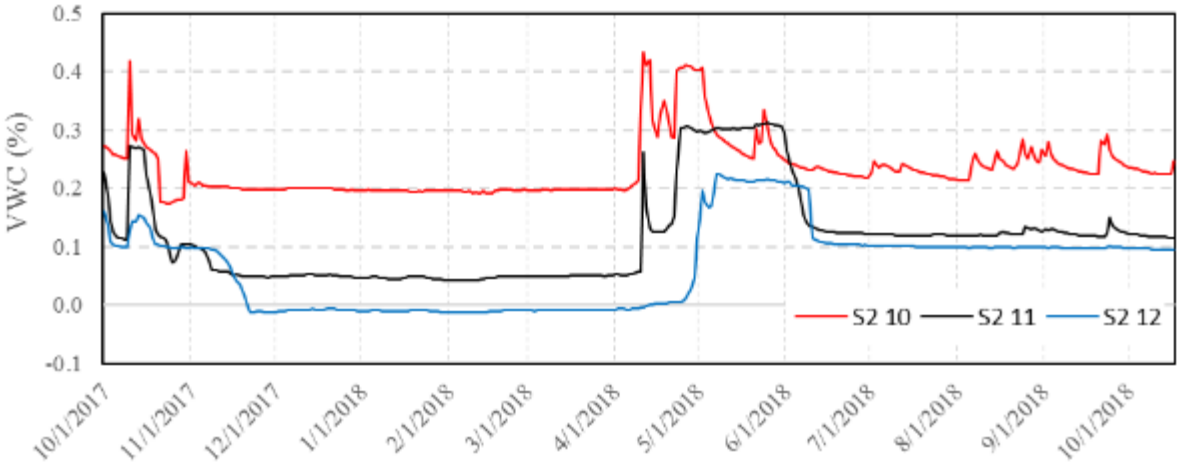

Figure A. 8 VWC at sensors 10 through 12 in section 2

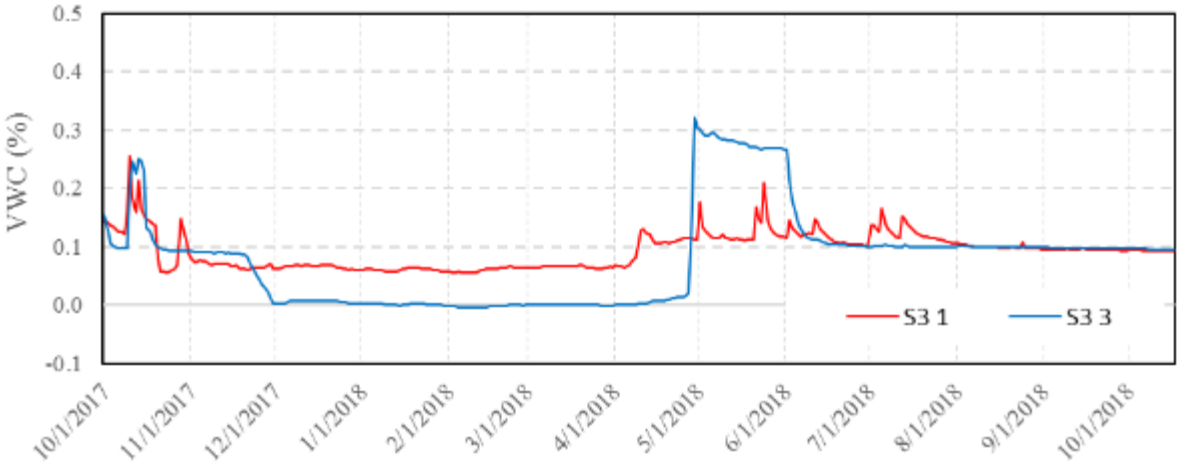

Figure A. 9 VWC at sensors 1 and 3 in section 3

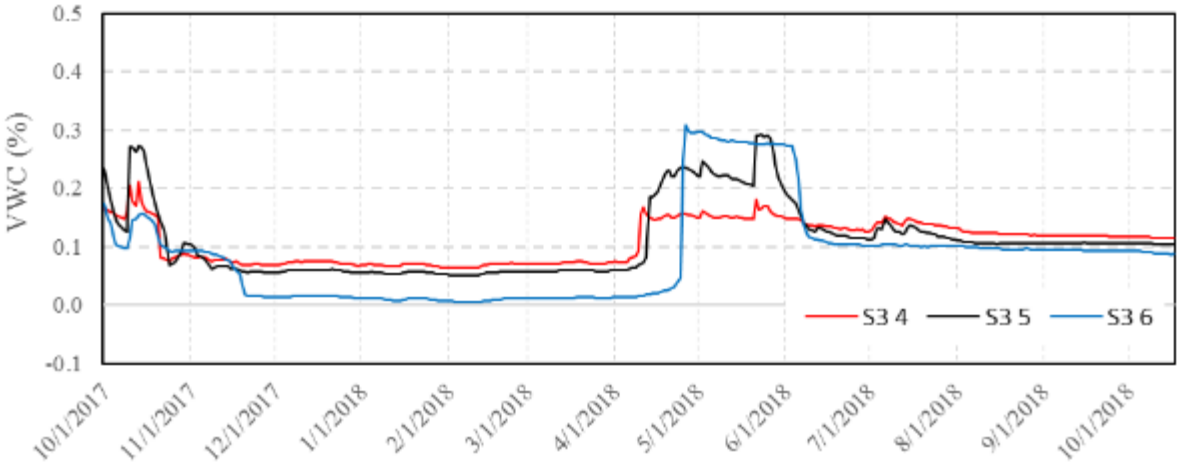

Figure A. 10 VWC at sensors 4 through 6 in section 3

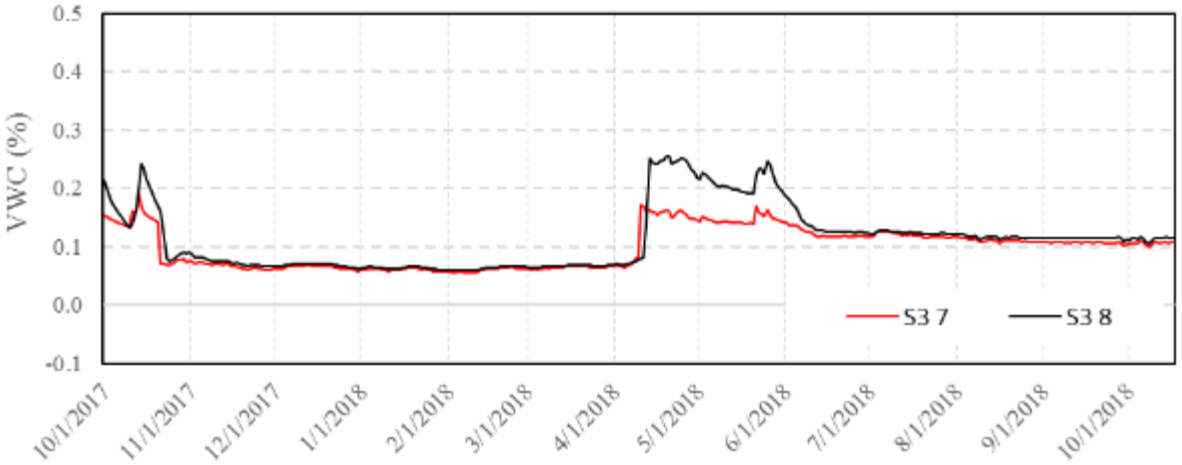

Figure A. 11 VWC at sensors 7 and 8 in section 3

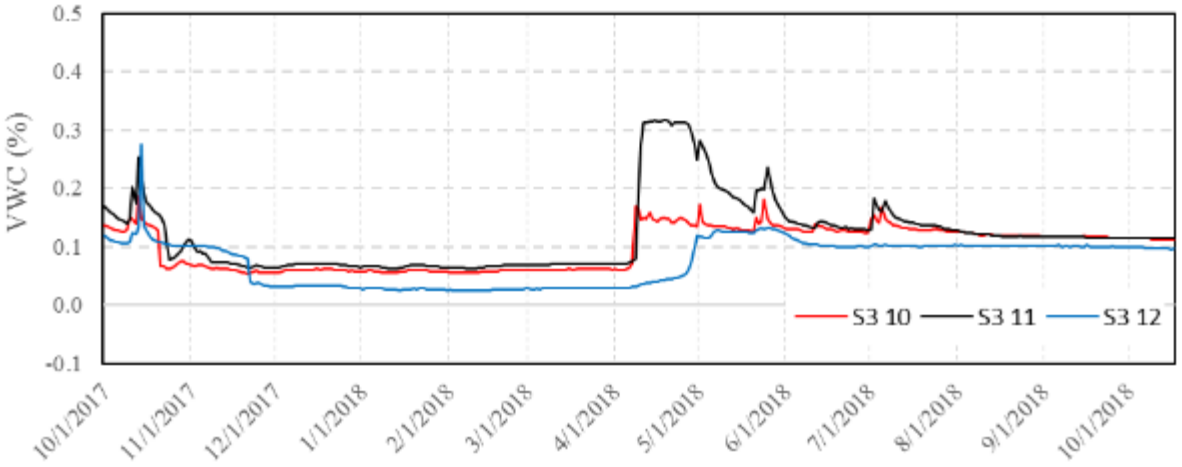

Figure A. 12 VWC at sensors 10 through 12 in section 3

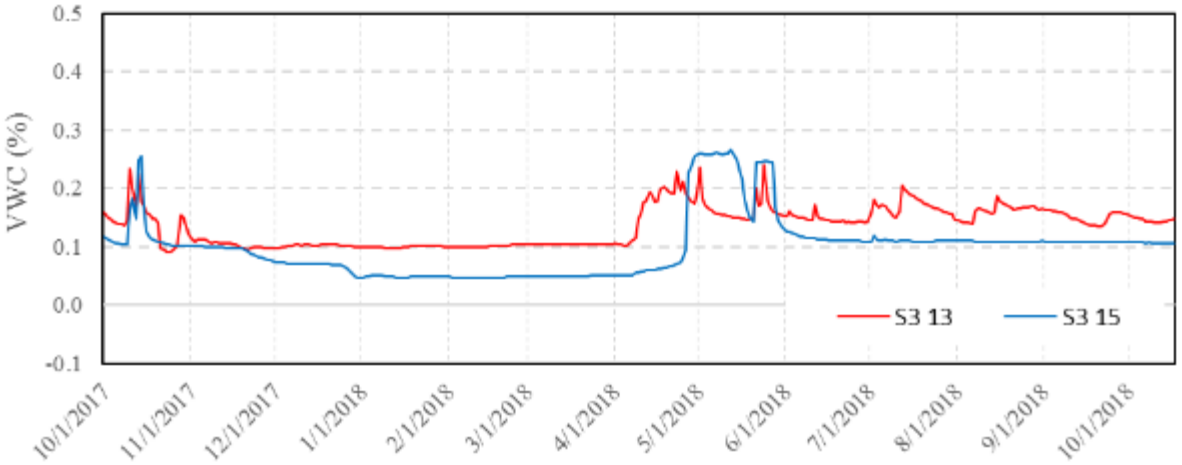

Figure A. 13 VWC at sensors 13 and 15 in section 3

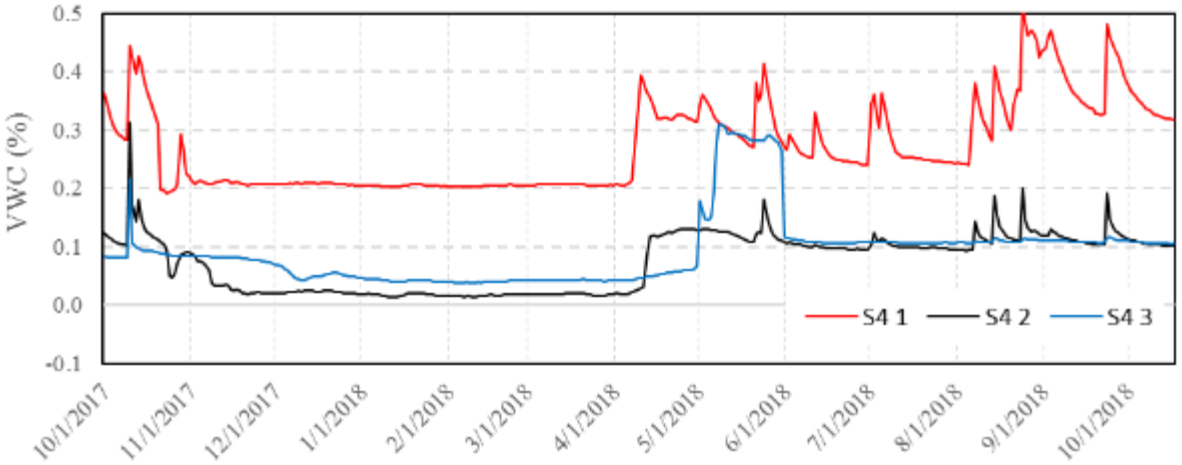

Figure A. 14 VWC at sensors 1 through 3 in section 4

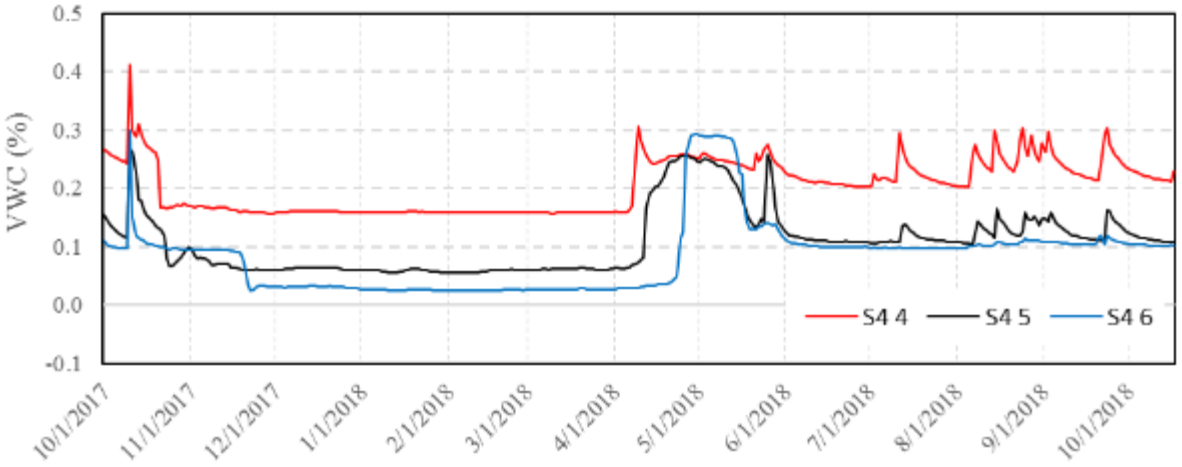

Figure A. 15 VWC at sensors 4 through 6 in section 4

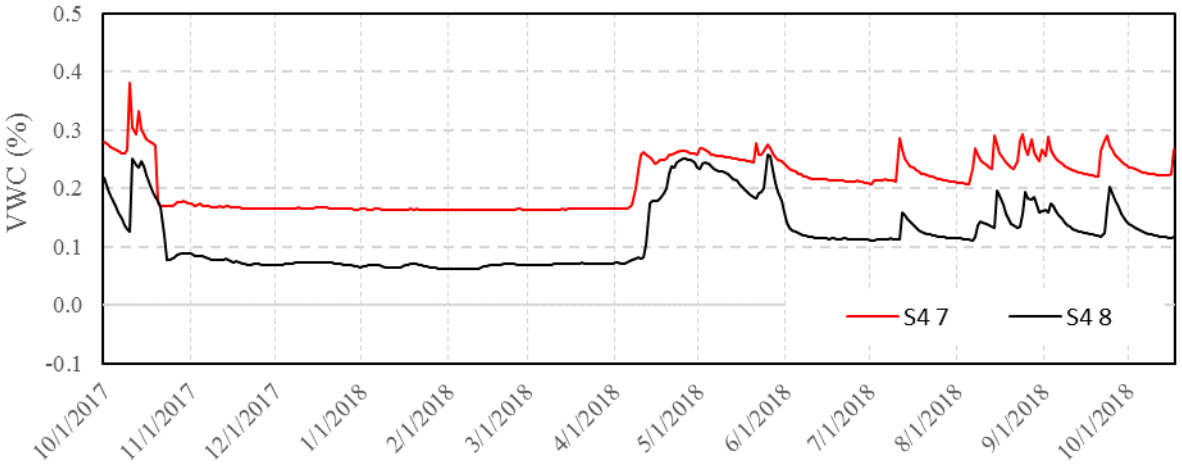

Figure A. 16 VWC at sensors 7 and 8 in section 4

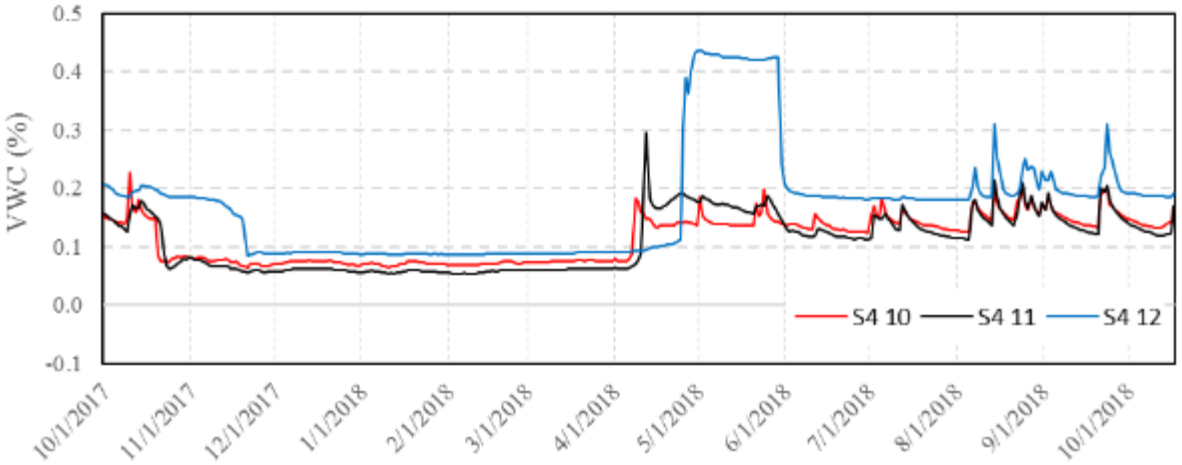

Figure A. 17 VWC at sensors 10 through 12 in section 4

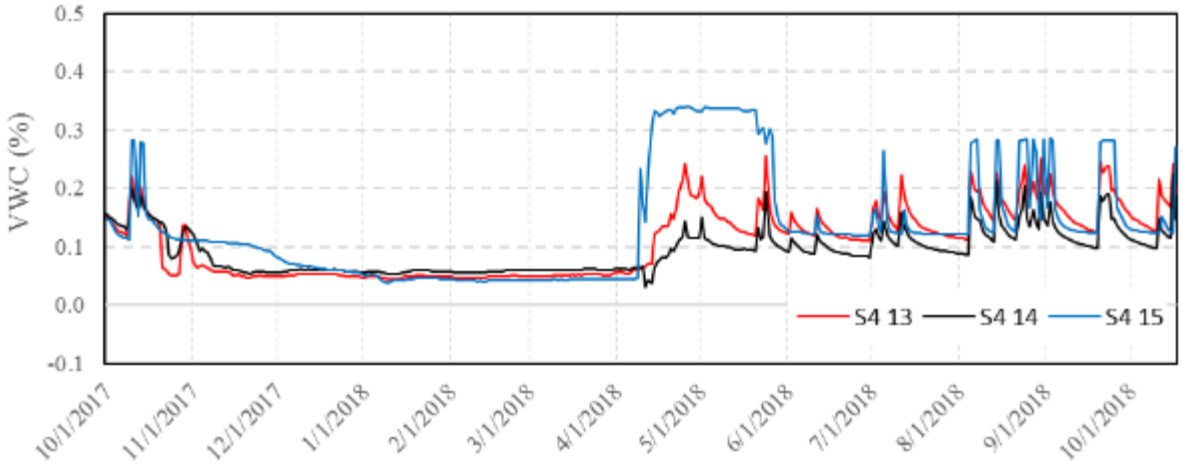

Figure A. 18 VWC at sensors 13 through 15 in section 4

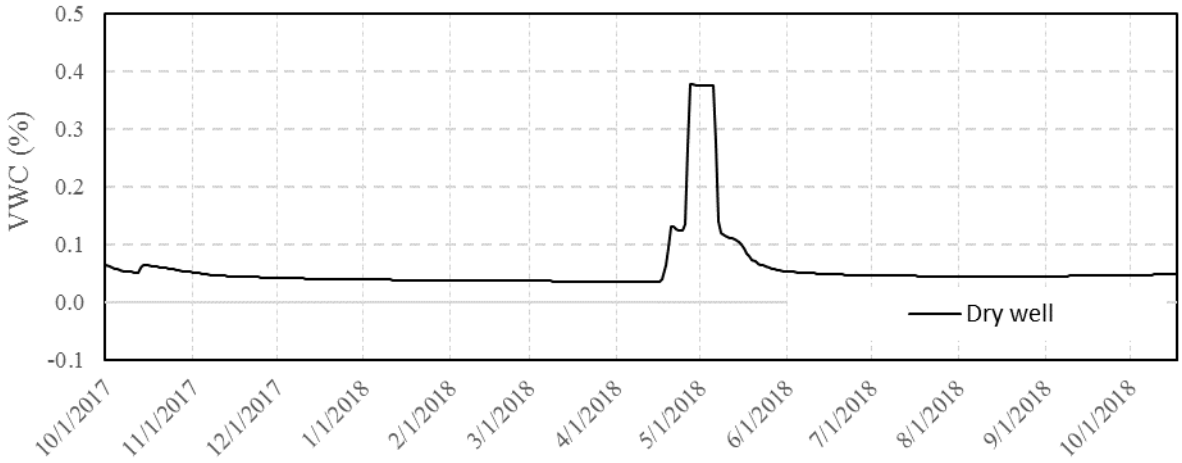

Figure A. 19 VWC at the dry well